Biophysical Journal Volume 109 December 2015 2574–2591

Article

Molecular and Mechanical Causes of Microtubule Catastrophe and Aging

Pavel Zakharov,[1] Nikita Gudimchuk,[2,3,4] Vladimir Voevodin,[3] Alexander Tikhonravov,[3] Fazoil I. Ataullakhanov,[2,3,4] and Ekaterina L. Grishchuk[1,*]

[1]Department of Physiology, Perelman School of Medicine, University of Pennsylvania, Philadelphia, Pennsylvania; [2]Center for Theoretical Problems of Physicochemical Pharmacology, Russian Academy of Sciences, Moscow, Russia; [3]Moscow State University, Moscow, Russia; and [4]Federal Research Center of Pediatric Hematology, Oncology and Immunology, Moscow, Russia

ABSTRACT Tubulin polymers, microtubules, can switch abruptly from the assembly to shortening. These infrequent transitions, termed "catastrophes", affect numerous cellular processes but the underlying mechanisms are elusive. We approached this complex stochastic system using advanced coarse-grained molecular dynamics modeling of tubulin-tubulin interactions. Unlike in previous simplified models of dynamic microtubules, the catastrophes in this model arise owing to fluctuations in the composition and conformation of a growing microtubule tip, most notably in the number of protofilament curls. In our model, dynamic evolution of the stochastic microtubule tip configurations over a long timescale, known as the system's "aging", gives rise to the nonexponential distribution of microtubule lifetimes, consistent with experiment. We show that aging takes place in the absence of visible changes in the microtubule wall or tip, as this complex molecular-mechanical system evolves slowly and asymptotically toward the steady-state level of the catastrophe-promoting configurations. This new, to our knowledge, theoretical basis will assist detailed mechanistic investigations of the mechanisms of action of different microtubule-binding proteins and drugs, thereby enabling accurate control over the microtubule dynamics to treat various pathologies.

INTRODUCTION

Microtubules (MTs), the cylindrical polymers of tubulin dimers, are a key component of the cytoskeleton. MTs have numerous cellular functions, including maintenance of cell architecture and intracellular transport, and they play an essential role in mitosis (1). MTs can exhibit sudden transitions between phases of slow growth and rapid shortening, and this dynamic behavior facilitates formation and positioning of the mitotic spindle and the search and capture of mitotic chromosomes. Moreover, MTs can work as molecular motors, producing mechanical work to move chromosomes (2). The dynamic instability of MTs can be observed in vitro in a reconstituted system containing soluble tubulin and GTP (3,4). During MT growth, tubulin dimers with the GTP-bound β-tubulin subunits are added to the tip of the MT, forming 13 parallel arrays called "protofilaments". This GTP becomes subsequently hydrolyzed, so the major part of the MT cylinder contains β-tubulins that are GDP-bound, while the newly added tubulin subunits form a so-called "GTP-cap" (5,6). The stochastic loss of the cap due to hydrolysis and subunit dissociation is thought to lead to a rapid transition from MT growth to shortening, termed "catastrophe". However, the mechanism of this transition and how it is linked to GTP hydrolysis is still unclear (7–10).

Since the discovery of MT dynamic instability, theoretical modeling of tubulin polymerization played a critical role in interpreting experimental observations and in defining the properties of the GTP-cap (6,11). The proposed models differ significantly in their frameworks, postulates, and mathematical approaches (11–20). Earlier models represented the MT with single or multiple protofilaments, describing their dynamics with kinetic constants that were different for GTP versus GDP-tubulin dimers. The two-state model by Hill (21), which additionally assumed random hydrolysis of the tubulin-bound GTP, simulated well the rate of tubulin de/polymerization as a function of soluble tubulin concentration. However, this and other kinetic models with random GTP hydrolysis (12,22) predicted a large GTP-tubulin cap and suggested that the cap-promoted stabilization should depend strongly on tubulin concentration (23). As a result, it has been difficult with this modeling framework to recapitulate two key experimental dependencies: a moderate suppression of MT catastrophe by increasing tubulin concentration (24,25); and the delay times in dilution experiments, in which MTs were first polymerized using different tubulin concentrations, then the free tubulin was removed rapidly (26,27). In the latter experiment, the MTs underwent catastrophes within 2–4 s after tubulin removal, and the delay time was only weakly dependent on the concentration of soluble tubulin. These experimental findings prompted development of the molecular-kinetic models with different GTP hydrolysis rules. For example, Bayley and colleagues (13,28,29) postulated that the GTP hydrolysis was not random but coupled to tubulin addition, thereby predicting a smaller GTP-cap that was not sensitive to tubulin concentration.

Importantly, these pioneering models were constructed when the high-resolution structure of the MT tip was still

Submitted June 16, 2015, and accepted for publication October 5, 2015.

*Correspondence: gekate@mail.med.upenn.edu

Editor: Stefan Diez.

0006-3495/15/12/2574/18

http://dx.doi.org/10.1016/j.bpj.2015.10.048

unavailable. These original and many subsequent molecular MT models did not incorporate tubulin conformation, which is different at the ends of growing versus shortening MTs (30,31), preventing these models from a realistic description of the evolving MT tip structure. Moreover, the ability of depolymerizing MTs to exert a large pulling force has also been documented only recently (32–34). Importantly, the proposed power-stroke mechanism of MT force generation imposes strong constraints on the possible MT energetics and mechanics (35). To describe these effects, a complex mechanical environment for all dimers at the MT tip should be considered, because GTP hydrolysis in one tubulin dimer induces a mechanical strain on its neighbors (9,36,37), affecting formation and breakage of the nearest and to a lesser degree more distant bonds. Recent molecular MT models have begun approaching this complexity by considering the energy of lateral and longitudinal tubulin-tubulin bonds (15) and approximating mechanical influences with the neighbor-specific kinetic rate constants (20). However, only with the development of molecular-mechanical MT models does it became possible to directly incorporate variable protofilament shapes by explicitly calculating bonds energies and elastic tubulin deformations, linking the behavior of the whole MT to the mechanics and energetics of its individual subunits. The molecular-mechanical model, constructed previously by our group, can successfully describe structural and mechanical properties of depolymerizing MTs, and, to our knowledge, is the only model today to describe quantitatively the generation of large pulling force by MT (17,34,38,39). However, all previous versions of this model did not include tubulin assembly, so its application to MT dynamic instability was not possible. The mechanochemical model, proposed by van Buren et al. (16), was the first molecular model to combine tubulin assembly, GTP hydrolysis, and tubulin bending, allowing its application to a broad range of experimental data. MT configurations in this model are calculated with a quasi-stationary approach, which combines equations of chemical thermodynamics and local energy minimization. Thermal fluctuations, however, are lacking, so the associated mechanical fluctuations of protofilament shape are not included. This model provides a good fit to various experimental findings, although it appears to predict an overly steep dependency of catastrophe frequency on tubulin concentration, while the ability of this model to describe the MT pulling force has not yet been established.

Understanding the molecular events that lead to catastrophe is additionally difficult because the stabilizing properties of the GTP-cap appear to change during MT lifetime, the phenomenon called “MT aging”. This slow evolution is evident from the nonexponential distribution of the MT lifetimes in vitro, consistent with a gradual increase in catastrophe frequency during the first few minutes of MT elongation (24,40). Two different MT models have so far been applied to describe this transient effect, leading to two different mechanisms to explain MT aging. In a kinetic multiprotofilament model by Bowne-Anderson et al. (11), the MT stochastically acquires permanent molecular hits, and the accumulation of three such hits is assumed to trigger a catastrophe (Fig. 1 *A*). Because these hits are irreversible and accumulate consecutively, this model predicts defects in the MT wall, e.g., elongated gaps in the walls of MT cylinder (11). Although there is currently no structural evidence to support presence of such massive visible alterations in the MT lattice, it is difficult to rule out that the slow accumulation of some less conspicuous but permanent abnormalities within the MT wall might cumulatively affect the structure or composition of the GTP-cap, and hence the frequency of catastrophe. In contrast, the mechanochemical model based on the work of van Buren et al. (16) predicts that during tubulin assembly, the wall of the MT polymer maintains its normal integrity, but the MT tips become more tapered with time, exhibiting an increasing mismatch in the length of individual protofilaments (Fig. 1 *B*) (41). This model therefore predicts visible aging of the MT tip structure, which increases catastrophe frequency during the first minutes of MT growth.

Importantly, while some theoretical models can recapitulate selected MT properties and experimental dependencies, it has not been possible so far to reproduce quantitatively all major kinetic, structural, and force generation properties of tubulin polymers within the frame of one model and one set of parameters, indicating that our understanding of the underlying molecular events is still incomplete. Here we report construction of a comprehensive molecular-mechanical model of the MT dynamics, which implements explicit Brownian dynamics simulation of tubulin-tubulin interactions. Brownian dynamics provides stochastic trajectories of tubulin monomers with high temporal resolution, while taking into account the mechanics of protofilament bending in a thermal bath. This contrasts the quasi-stationary thermodynamic approach, in which system behavior is approximated with a series of computational steady-state steps in the absence of thermal fluctuations; because the evolving MT tip system is far from equilibrium, the quasi-stationary approach may not be adequate. To simulate Brownian dynamics on the experimentally relevant timescale, we conducted massive parallel computations using the Lomonosov supercomputer at the Moscow State University (0.9 PFlops Linpack Performance) (42). Strikingly, this approach led to an overall good quantitative agreement between the model and major experimental characteristics of the dynamic MTs. We have dissected detailed molecular events that precede and accompany the MT catastrophe in silico to derive a comprehensive description of the underlying mechanisms and their timescales. We show that MT catastrophe results from random fluctuations in the number and extent of protofilament bending, not just in the size of the GTP-cap at a growing tip. Importantly, MT aging in the model is not caused by a permanent change in the MT wall or tip tapering, but it is driven by the slow evolution of stochastic

reversible events that take place continuously at the growing MT end.

MATERIALS AND METHODS

Model description

Model geometry

MT is modeled as a cylindrical array of tubulin dimers arranged into 13_3 lattice with the plus MT end pointing upward (see Molodtsov et al. (17) for details). Position and orientation of each tubulin monomer in the lattice is fully defined by three coordinates (x_i, y_i, τ_i), where x_i and y_i are positions of the center of the subunit, and τ_i is the orientation angle. Monomers interact at four contact points with the neighboring subunits: there are two longitudinal and two lateral bonds per monomer (Fig. 1 *C*; and see Efremov et al. (39) for details). Different forms of tubulin, containing GTP or GDP, are modeled similarly but with different values of model parameters (as described below). Free soluble tubulin dimers can incorporate into MT by attaching longitudinally at the MT end. Importantly, the model does not describe any motions or changes in conformation of soluble tubulins, and calculations begin after the GTP dimer has formed the MT end attachment and adopted the straight configuration (see *Choice of Model Parameters and Model Calibration* later in the text). For simplicity, we assume that binding occurs with equal probability to any terminal dimer, independently of its nucleotide state or location. Although local structure can sterically inhibit subunit association, a prior theoretical model finds that the global structure of the tip is unlikely to affect the association rate to lagging versus leading protofilaments (43).

Energy potentials for tubulin-tubulin interactions within the MT wall and protofilament bending

Lateral interaction between each pair of adjacent tubulin monomers is described with the energy potential v^{lat} that contains a quadratic well and a repulsion barrier (Fig. 1 *C*):

$$v^{\text{lat}}_{k,n}(r_{k,n}) = A_{\text{lat}} \times \left(\frac{r^{\text{lat}}_{k,n}}{r_o}\right)^2 \times \exp\left(\frac{-r^{\text{lat}}_{k,n}}{r_o}\right) - b_{\text{lat}} \times \exp\left(\frac{-\left(r^{\text{lat}}_{k,n}\right)^2}{d \times r_o}\right). \quad (1)$$

Here, $r^{\text{lat}}_{k,n}$ is the distance between two adjacent lateral interaction points between the kth tubulin monomers located in the protofilaments n and $n+1$. See Fig. S1 *A* in the Supporting Material, *Choice of Model Parameters and Model Calibration* later in the text, and Table 1 for description of other model parameters.

Longitudinal bonds between tubulin monomers are modeled differently, depending on whether they are inter- or intradimer bonds. The interdimer bonds between the tubulin monomers that belong to adjacent, head-to-tail attached dimers are described analogously to the lateral bonds:

$$v^{\text{inter}}_{k,n}(r_{k,n}) = A_{\text{inter}} \times \left(\frac{r^{\text{inter}}_{k,n}}{r_o}\right)^2 \times \exp\left(\frac{-r^{\text{inter}}_{k,n}}{r_o}\right) - b_{\text{inter}} \times \exp\left(\frac{-\left(r^{\text{inter}}_{k,n}\right)^2}{d \times r_o}\right). \quad (2)$$

Here, $r^{\text{inter}}_{k,n}$ is the distance between two adjacent longitudinal interaction points between tubulin monomers k and $k+1$, located in protofilament n between two dimers; parameters r_o and d are the same for lateral and longitudinal bonds. All parameters in Eqs. 1 and 2 are the same for GTP- and GDP-tubulins.

The intradimer longitudinal bonds (between the monomers within one dimer) are unbreakable, modeled as Hookean springs with stiffness k:

$$v^{\text{intra}}_{k,n}(r_i) = \frac{1}{2}k \times r^2_{k,n}. \quad (3)$$

Here, $r_{k,n}$ is the distance between two adjacent longitudinal interaction points between monomers within one tubulin dimer.

In addition to the energy of molecular bonds between tubulin monomers, the model also takes into account the energy associated with protofilament's bending. In the model, the bending takes place via the subunits rotation at the longitudinal interaction points between monomers that belong to the same protofilament, which curls in the plane defined as in Molodtsov et al. (17). Protofilament bending energy g^{bending} depends on angle $\chi_{k,n}$ between the adjacent monomers in the plane of this protofilament:

$$g^{\text{bending}}_{k,n} = \frac{B}{2}\left(\chi_{k,n} - \chi_o\right)^2. \quad (4)$$

Here, $\chi_{k,n} = (\tau_{k,n} - \tau_{k-1,n})$ is the angle between k and $k-1$ monomers in the protofilament n; the $\tau_{k,n}$ value is the angle formed between this monomer and the MT axis; and χ_o is either $\chi^D{}_o$ or $\chi^T{}_o$, depending on the associated nucleotide GDP or GTP, respectively. See *Choice of Model Parameters and Model Calibration* later in the text and Table 1 (and see Müller-Reichert et al. (44) and Melki et al. (45)) for description of other parameters.

The total energy of the MT, U_{total}, is given by the sum of all its components:

$$U_{\text{total}} = \sum_{n=1}^{13}\sum_{k=1}^{K_n}\left(v^{\text{lat}}_{k,n} + v^{\text{inter}}_{k,n} + v^{\text{intra}}_{k,n} + g^{\text{bending}}_{k,n}\right). \quad (5)$$

Here, K_n is the total number of tubulin subunits in the nth protofilament.

Numerical calculations

The computer code was written in C++ and parallelized with OpenMP. The algorithm consisted of two parts: the dynamic part describing the molecular dynamics of polymerized tubulin monomers and the kinetic part for a stochastic association of new tubulin dimers at the ends of MT protofilaments.

The dynamic part of our algorithm calculates tubulin monomer coordinates in space and time using a Brownian dynamics approach described in Ermak and McCammon (46). Briefly, the initial configuration is an MT seed of 10 tubulin monomers in length. The coordinates of these monomers are used as initial conditions for Langevin equations to calculate new coordinates for all subsequently added tubulin monomers. The coordinates of the system at the ith computation cycle are given by

$$\begin{cases} q^i_{k,n} = q^{i-1}_{k,n} - \dfrac{dt}{\gamma_q} \times \dfrac{\partial U_{\text{total}}}{\partial q^i_{k,n}} + \sqrt{2k_{\text{B}}T\dfrac{dt}{\gamma_q}} \times N(0,1) \\ \tau^i_{k,n} = \tau^{i-1}_{k,n} - \dfrac{dt}{\gamma_\tau} \times \dfrac{\partial U_{\text{total}}}{\partial \tau^i_{k,n}} + \sqrt{2k_{\text{B}}T\dfrac{dt}{\gamma_\tau}} \times N(0,1) \end{cases}, \quad \gamma_q = 6\pi r\eta, \quad \gamma_\tau = 8\pi r^3\eta. \quad (6)$$

TABLE 1 Model Parameters

Parameter	Description	Value	Comments
r_o	width of energy potential well, characterizing the length of tubulin-tubulin bond	0.12 nm	see *Choice of Model Parameters and Model Calibration* in the text
d	shape parameter	0.25 nm	
A_{lat}	corresponds approximately to 2× height of the energy barrier for a lateral bond	16.9 k_BT	
b_{lat}	depth of the energy potential well for a lateral bond	9.1 k_BT	
A_{inter}	corresponds approximately to 2× height of the energy barrier for longitudinal interdimer bond	17.6 k_BT	
b_{inter}	depth of the potential well for longitudinal interdimer bond	15.5 k_BT	
k	stiffness of longitudinal intradimer bond	517 k_BT nm^{-2}	
B	flexural rigidity of protofilament bending	300 k_BT rad^{-2}	(39)
$\chi^D{}_o$	equilibrium angle between longitudinally attached GDP-tubulin monomers	0.2 rad	(44)
$\chi^T{}_o$	equilibrium angle between longitudinally attached GTP-tubulin monomers	0 rad	$0 < \chi^T{}_o < 0.09$ (37,44)
c_{tub}	soluble tubulin concentration	6–20 μM	experimental range in vitro
$k_{on,MT}$	on-rate constant for tubulin addition per MT	8.3 μM^{-1} s^{-1} (6.4 s^{-1} per protofilament at 10 μM tubulin)	see *Choice of Model Parameters and Model Calibration* in the text
K_{hydrol}	rate of GTP hydrolysis normal	0.5 s^{-1}	(45)
	accelerated	9 s^{-1}	this model
T	temperature	300 K	this model
η	viscosity	0.2 Pa·s	this model
dt	time step for dynamic algorithm	2 × 10^{-10} s	this value enables convergence of calculations
t_{kin}	time step for kinetic algorithm	10^{-3} s	this model

See Fig. S1 *A* for illustration of bond energy characteristics.

Here, $q_i = \{x_i, y_i\}$; dt is the time step; U_{total} is given by Eq. 5; γ_q and γ_τ are translational and rotational viscous drag coefficients, respectively, calculated for a sphere with radius $r = 2$ nm; k_B is the Boltzmann constant; T is the temperature; and $N(0,1)$ is a random number from the normal distribution. The gradients $\partial U/\partial q_i$ were calculated as described in Appendix SA.

A tubulin dimer was considered detached (and was no longer simulated) when the distance between its lower longitudinal binding site and the upper longitudinal binding site on the neighboring dimer in the same protofilament exceeded 1 nm. This separation threshold corresponds to a negligible energy of interaction between two proteins. To speed up calculations, and unless stated otherwise, the dynamic algorithm was applied to all dimers located four layers below the terminal dimer of the shortest protofilaments and to all GTP-dimers located elsewhere in the MT wall, but the coordinates of other tubulins in the cylindrical part of the MT were not updated. This simplification is justified by our prior analysis in Molodtsov et al. (17), where changes in the coordinates of one tubulin dimer in the cylindrical part of the MT were found to have mostly a local effect, influencing the dimers in the immediate vicinity but not elsewhere in the MT wall.

The kinetic part of the algorithm describes the incorporation of new tubulin dimers at the MT end. A new tubulin dimer attaches to any of the MT-terminal tubulins every millisecond of the model time with probability p:

$$p = k_{on,MT} \times c_{tub} \times t_{kin}. \quad (7)$$

Here, $k_{on,MT}$ is the on-rate constant for tubulin subunits addition to the MT, c_{tub} is the concentration of soluble tubulin, and t_{kin} is the time step for the kinetic algorithm.

This algorithm was implemented by comparing the probability of attachment p with random numbers p_j from even distribution for interval [0,1] generated for each MT protofilament. A new GTP-tubulin dimer was added to the nth protofilament when $p_n < p$. The coordinates (x_i, y_i, τ_i) of the newly added dimer were assigned such that it formed the unstressed longitudinal bond with its bottom neighbor ($\chi_o{}^T = 0$); see *Choice of Model Parameters and Model Calibration* later in the text. After the GTP-tubulin dimer was incorporated, GTP hydrolysis in this dimer occurred stochastically with the rate constant K_{hydrol} implemented as above: a random number p_k was generated from the even distribution [0,1] for every GTP-tubulin in the MT once per millisecond. A typical simulation of 1 s of MT dynamics took 25–30 h. The calculation results were processed in MATLAB 2012b (The MathWorks, Natick, MA) (see Appendix SB and Fig. S2).

Choice of model parameters and model calibration

As in our previous versions of molecular-mechanical model, we assume that the equilibrium conformation for the GDP-tubulin incorporated into the MT wall is bent with equilibrium angle of 0.2 rad between the head-to-tail attached monomers, consistent with the structure of ram's-horns at the end of the depolymerizing MT (30,44). The equilibrium conformation for the GTP-tubulin in the polymerized state is known with less certainty. It has been suggested that soluble GTP-tubulin attaches to the MT tip in a fully bent conformation (0.2 rad), but then it adopts a smaller bending angle (47). However, the exact angular change, timing for this transition,

and whether it is caused by the longitudinal or the lateral bonds or both, or by the allosteric effects, is not yet known (48), preventing us from incorporating these transitions explicitly in a justifiable manner. Even more impeding is the lack of knowledge about the bending rigidity of the soluble GTP-tubulin dimer. If we assume that GTP- and GDP-bound soluble tubulins have the same bending rigidity (as assumed for the polymerized tubulins in our model) and that they have the same equilibrium angle (0.2 rad), MT polymerization is not possible in our model, despite our use of the high energy lateral and longitudinal bonds (Table 1, see below). This result does not argue against the idea that GTP-tubulin straightens at the MT tip but it highlights the difficulties of modeling such a transition until a strong, quantitative experimental base is established. In this model, we begin calculations of MT dynamics downstream from a presumptive phase of GTP-tubulin straightening. The equilibrium angle for the polymerized GTP-tubulin can be estimated to be ~0.09 rad from the GMPCPP-containing tubulin structures (37,44). Our previous theoretical analysis of the impact of this angle on MT stability shows little effect for the angular range of 0–0.05 rad (17). Here, for simplicity, we use the 0 rad angle, but model results do not change significantly in the above angular range. Future modeling should explore larger equilibrium angles for soluble and polymerized GTP-tubulin and a range of GTP-tubulin stiffnesses to enable the incorporation of conformational transitions during early steps of tubulin addition.

The flexural rigidity of protofilament bending B was estimated as in the previous versions of the molecular-mechanical model (17,38,39). Briefly, the entire energy of GTP hydrolysis is assumed to be stored in the strained conformation of a polymerized GDP-tubulin dimer. Under this assumption, the maximal thermodynamically possible force that the MT can generate is ~80 pN, but biomechanically different couplers transduce the force of bending protofilaments with different efficiency (34). Importantly, the MT depolymerization force is proportional to B, so smaller B implies a smaller predicted force. The value of B in our model lies in the range of the protofilament bending stiffness determined from nanoindentations in silico (49). We also assume that the protofilament stiffness is the same for GDP- and GTP-tubulins (50). The value of k, stiffness of longitudinal intradimer bond, was chosen such that inter- and intradimer bonds had similar rigidity. The soluble tubulin concentration c_{tub} was varied in the range typical for experiments in vitro (24,25). The parameter K_{hydrol} for simulations of MT growth and shortening (see Figs. 2, 4 *B*, 5, and 6) was 0.5 s^{-1}, which represents the upper boundary for an estimated GTP hydrolysis rate in vitro (45). MT catastrophe calculations were done using $K_{hydrol} = 9\ s^{-1}$, and these data were normalized (see Figs. 3, 4, 7, and S3 and Appendix SC), except in Fig. 7, *A* and *B*, which shows plots for $K_{hydrol} = 9\ s^{-1}$ without the normalization.

Model calibration, during which the values of other unknown parameters for tubulin-tubulin interaction are defined, is based on the experimental evidence that during MT disassembly the lateral bonds dissociate before the longitudinal ones (52), implying that the rate of MT disassembly is determined primarily by the characteristics of the lateral bonds. Previously estimated A_{lat} (17) was used as an initial value to find A_{lat} and b_{lat} that in this model give the average MT disassembly rate 24 μm/min, similar to the experimentally observed MT shortening rate in vitro (25). The value of A_{inter} was chosen roughly similar to A_{lat}; these parameters define the height of energy barrier for the respective bond (see Fig. S1 *A*). After the values of parameters A_{lat}, b_{lat}, and A_{inter} were fixed, the values of parameters $k_{on,MT}$ and b_{inter} for the longitudinal bond were chosen to achieve a fit to the experimental dependence of MT growth rate on tubulin concentration (Fig. 2 *B*) (25). The resulting values of b_{lat} and b_{inter} used in this model are similar to the intertubulin bond energies estimated from the coarse-grained molecular dynamic simulations of MT nanoindentations (49). Importantly, our model assigns the same bond energies for the GTP- and GDP-tubulins (Table 1), consistent with a recent structural study (9) and our prior theoretical finding that weakening lateral bonds have little effect on MT shape and stability (17). The effect of the shape of energy potential and parameter r_o have been explored by us previously (17,38,39); $r_o = 0.12$ nm and $d = 0.25$ nm appear to be optimal for modeling interactions in the presence of thermal fluctuations. See Appendix SD for additional information about these parameters values and how they differ from those used in the mechanochemical models.

RESULTS

Construction of the molecular-mechanical model of the dynamic MT

Our model combines the traditional kinetic approach to tubulin assembly and the explicit Brownian dynamics simulations of tubulin-tubulin interactions. Tubulin monomers are used as unit structures; GTP tubulin dimers bind to the tips of the 13 protofilament helical MT at the millisecond timescale, characterized by the rate constant $k_{on,MT}$ (Fig. 1 *C*). To describe tubulin interactions, we employ the simplest assumptions, so that the baseline behavior of this model can be established before exploring additional complexities and modifications. For GTP hydrolysis, we assume that after tubulin association, the GTP is hydrolyzed randomly regardless of this dimer's location. GDP-tubulins in the MT wall tend to adopt a bent conformation, consistent with the structure of curved tubulin protofilaments at the end of the depolymerizing MT (30,44). The interactions between the GTP- and GDP-containing tubulin subunits in the MT wall are defined with specific energy potentials, similarly to other molecular-mechanical models (16,17,39). Lateral and longitudinal bonds between tubulin dimers can stretch and break if the energy barriers are exceeded, but the energy profiles are assumed to be same for GDP- and GTP-tubulins. To our knowledge, the major novel feature of our approach is that all molecular-mechanical interactions between tubulin monomers within the MT wall and at the tip, including formation and rupture of bonds, are determined explicitly by solving Langevin equations of motion. Thus, the model does not assume any specific dissociation rate constant, but the tubulins dissociate only owing to the dynamic evolution of this complex system. Consequently, there are no thermodynamic penalties or imposed rules for tubulin dimers dissociation depending on their specific location or identity of their neighbors within the tip. MT catastrophe in this model is, therefore, a natural result of the structure and energetic of the polymer configurations, and the model contains no artificially introduced catastrophe-promoting or -inhibiting features.

Configuration of the MT lattice and its tip were determined with a 200-ps time step (42). During one computing step, the model calculates spatial and angular coordinates for up to 300 tubulin dimers at the MT plus-end. It takes 70–100 h to calculate 3 s of MT lifetime. The complete model contains 17 parameters (Table 1); detailed model description and calculation algorithms are provided in the first two subsections under Materials and Methods. Values of some model parameters, e.g., the typical length of a protein-protein bond, were taken or estimated by us based on

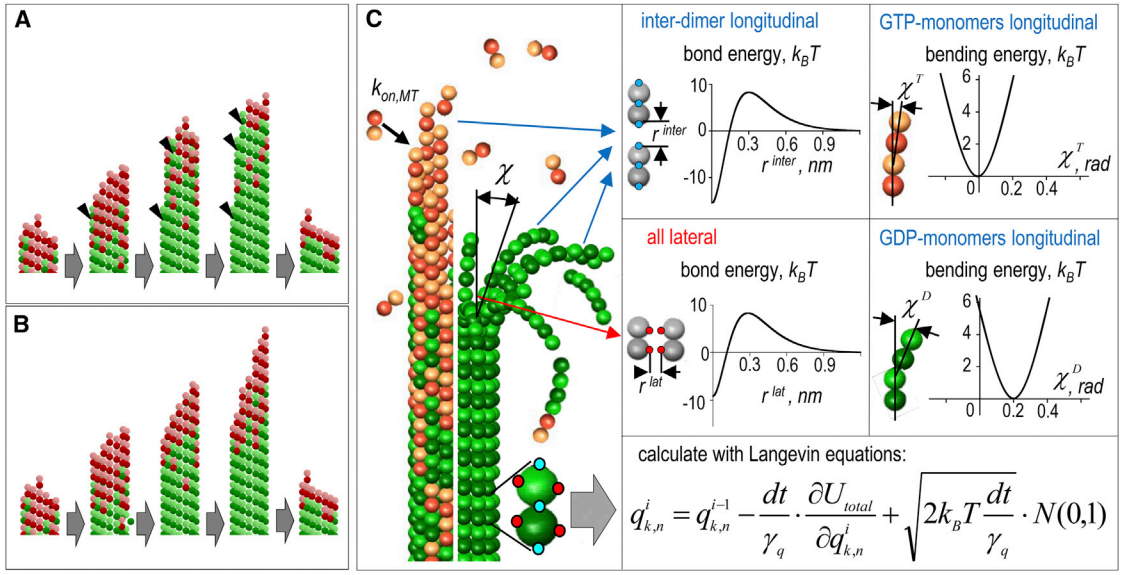

FIGURE 1 Theoretical models to study age-dependent MT catastrophes. (*A*) Simplified schematics of the MT aging mechanism, in which catastrophe is triggered by the accumulating permanent catastrophe-promoting defects in the MT wall (*arrowheads*). (*B*) Simplified schematics of the MT aging mechanism, in which the MT tip ages due to the persistent increase in the tip's tapering. (*C*) Diagram depicting essential features of the molecular-mechanical model, in which tubulin monomers in the MT wall interact with each other via two lateral and two longitudinal bonds with specified energy potentials. (*Brown*) GTP-bound dimers; (*green*) GDP-dimers. See Materials and Methods for details. To see this figure in color, go online.

Molodtsov et al. (17) and Efremov et al. (39). Those parameters that are currently not known were fitted with the model (see *Choice of Model Parameters and Model Calibration* earlier in the text). After all model parameters were specified, their values were fixed (Table 1) and the resulting model behavior was examined.

Molecular-mechanical model recapitulates major kinetic and structural features of the dynamic MTs

Typical calculation of MT dynamics started from a short MT seed (see Movie S1), in which GTP was nonhydrolyzable and longitudinal bonds were unbreakable; this configuration is similar to the GMPCPP-MT seeds used in vitro. MT elongation from the seed proceeded steadily at ~2 μm/min for 10 μM tubulin (Fig. 2 *A*) and the rate increased with increasing concentration of soluble tubulin in a good agreement with experiment (Fig. 2 *B*). The configuration of MT ends during polymerization was similar to those reported with electron microscopy for this tubulin concentration range: the growing MT tips were fairly straight, with no highly elongated protrusions (Fig. 2 *C*) (30,31). The tips contained a mixture of tubulins in GTP- and GDP-configurations, and the GTP-tubulin islands were seen occasionally in the MT wall (53). The shape of the shortening MT tips in the model was dramatically different from that of the growing tips (Fig. 2 *D*; and see Movie S1). Moreover, the shape of curled protofilaments in silico was in a quantitative agreement with the ram's-horns seen in electron micrographs of the MTs depolymerizing in vitro (52) (Fig. 2 *E*). The distributions of the length of real ram's-horns and of those in the model were also similar (Fig. 2 *F*). This match has not been seen with previous molecular-mechanical models, in which the length of protofilament curls was either too short (16) or fixed artificially (39,51). The average rate of MT shortening in silico was 24.4 $\pm$ 4.4 μm/min (mean $\pm$ SD, $N = 16$) and it varied considerably not only from one simulated MT to another, but also during the shortening of one MT (Fig. 2 *G*), as seen in the experiment (54). The rate of MT shortening in vivo and in silico showed no significant dependency on tubulin concentration (Fig. 2 *H*). Thus, this model can recapitulate major aspects of the MT assembly and disassembly.

The model predicts a nonexponential distribution of MT lifetimes

The stochastic transitions from MT growth to shortening in vitro are infrequent: 0.001–0.005 s^{-1} (24,25). Even with the use of a supercomputer and parallel programming, as of this writing, it is not possible to examine within a reasonable timeframe the events that are so infrequent. To overcome this technical limitation we sped up the acquisition of MT lifetime statistics using an increased rate of GTP hydrolysis. When GTP hydrolysis was accelerated 6–18-fold, spontaneous MT catastrophes were observed, as shown in Movie S3, which depicts 6.8 s of the MT lifetime and corresponds to the computing time of ~170 h. The resulting catastrophe frequency was proportional to the rate of GTP hydrolysis (Fig. 3 *A*), so the acquired MT catastrophe rates and lifetimes were normalized to compare with experimental data in vitro. This scaling procedure is

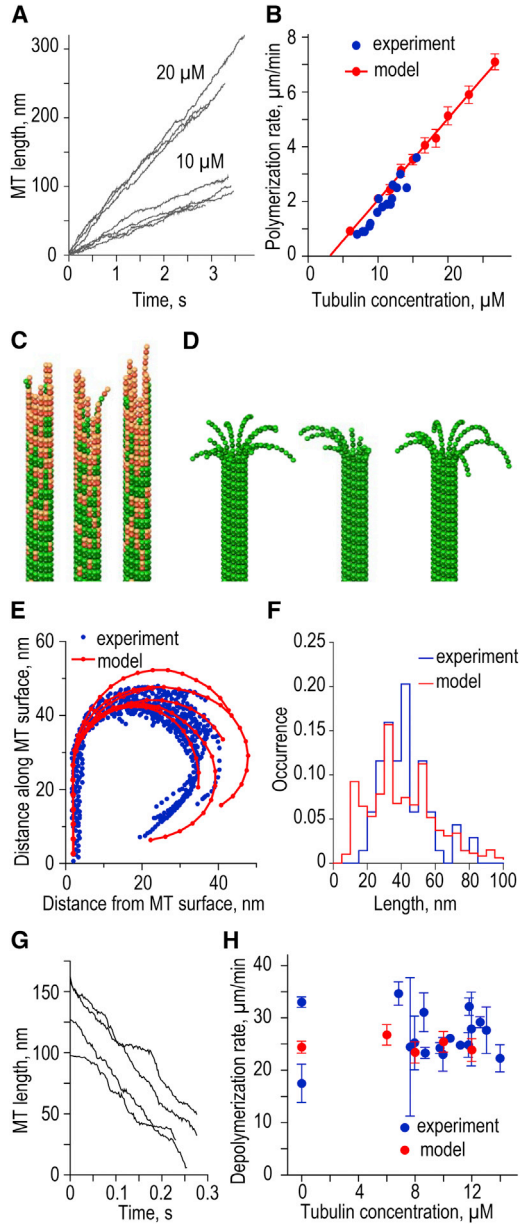

FIGURE 2 Modeling results for MT kinetics and overall tip structure. (*A*) Typical length versus time plots for in silico MTs growing at two soluble tubulin concentrations. Each curve represents the results of one simulation sampled with a 2 ms interval with no smoothing. All data here and in other figures were obtained with model parameters as in Table 1, unless specified otherwise; all panels in this figure are for $K_{hydrol} = 0.5\ s^{-1}$. (*B*) Dependence of the MT growth rate on soluble tubulin concentration. Experimental data from Walker et al. (25). Each theoretical data point is the mean of 8–16 repeats; bars are SDs. (*C*) Typical configurations of the growing MT tips in silico (10 μM tubulin). The growing tips are straight and contain several protofilament extensions, typically 3–4 tubulin dimers in length. (*D*) Typical configurations of the shortening MT tips in silico (0 μM tubulin). (*E*) Tracings of the curled protofilaments at the ends of shortening MTs in silico versus in vitro (in vitro data are from Mandelkow et al. (30), as analyzed in McIntosh et al. (51)). (*F*) Length distributions of the curled protofilaments in silico versus in vitro. The average protofilament length (mean ± SD) is 39 ± 21 nm ($N = 12{,}861$) and 40 ± 15 nm ($N = 72$), respectively. See legend to (*E*). (*G*) Typical length-versus-time plots for the shortening MTs in silico. Each curve represents results of an individual MT simulation, which was sampled with a 2 ms interval and displayed with no smoothing. (*H*) Dependence of the MT shortening rate on soluble tubulin concentration. Theoretical data points show mean ± SE based on $N \geq 6$ simulations for each tubulin concentration. Experimental data with soluble tubulin are from Walker et al. (25); two data points with zero soluble tubulin are from Walker et al. (27) and Tran et al. (52). To see this figure in color, go online.

justified by our findings that the normalized MT lifetime distributions obtained with different hydrolysis rates were similar, and that other quantitative parameters describing the shape of a growing tip also scaled linearly with increasing hydrolysis rate (see Fig. S3 and Appendix SC). Using this approach, we found that the MT catastrophe frequency in the model changed only weakly with tubulin concentration (Fig. 3 *B*). Although this prediction is in tune with the experimental data from several studies (Fig. 3 *B*), this modeling result is unexpected because random GTP hydrolysis has been suggested to lead to a sharp dependency (11). We note that this previous conclusion was reached using a modeling approach that lacked mechanical aspects of tubulin-tubulin interactions, so apparently this conclusion cannot be extended to the models with Langevin dynamics.

We then examined $N = 113$ dynamic MTs, recording their elongation time before catastrophe. Strikingly, the resulting distribution of the MT lifetimes was not exponential (Fig. 3 *C*). Correspondingly, the catastrophe frequency increased with characteristic time ~160 s, providing a good fit to the experiment (Fig. 3 *D*). Furthermore, in our model the increasing tubulin concentration had a stronger effect when catastrophe frequency was plotted as a function of the MT length, rather than lifetime (Fig. 3, *E* and *F*), as reported from in vitro experiments (24,40). Therefore, the MT dynamics in our model exhibits the main quantitative features that define MT aging in vitro.

MT aging in silico is not caused by the accumulation of permanent defects in the MT wall

One previous model to explain MT aging postulates that the walls of the growing MTs change physically during polymerization, leading to a gradual accumulation of the memorized defects in the MT wall and tip, eventually triggering the catastrophe (Fig. 1 *A*) (11). To investigate whether such a mechanism was at work in our model, we visually examined the walls of the growing MTs in silico, but found no evidence for the age-related alterations or irregularities in the tubulin lattice. All polymers that experienced catastrophes had 13 cylindrically arranged protofilaments, and their walls were visibly similar to those in the stable MT seeds. We also note that our model contains no artificially introduced defects that could be linked to a catastrophe. Additionally, we examined catastrophes in the polymers, in which a lower portion of the wall cylinder was frozen,

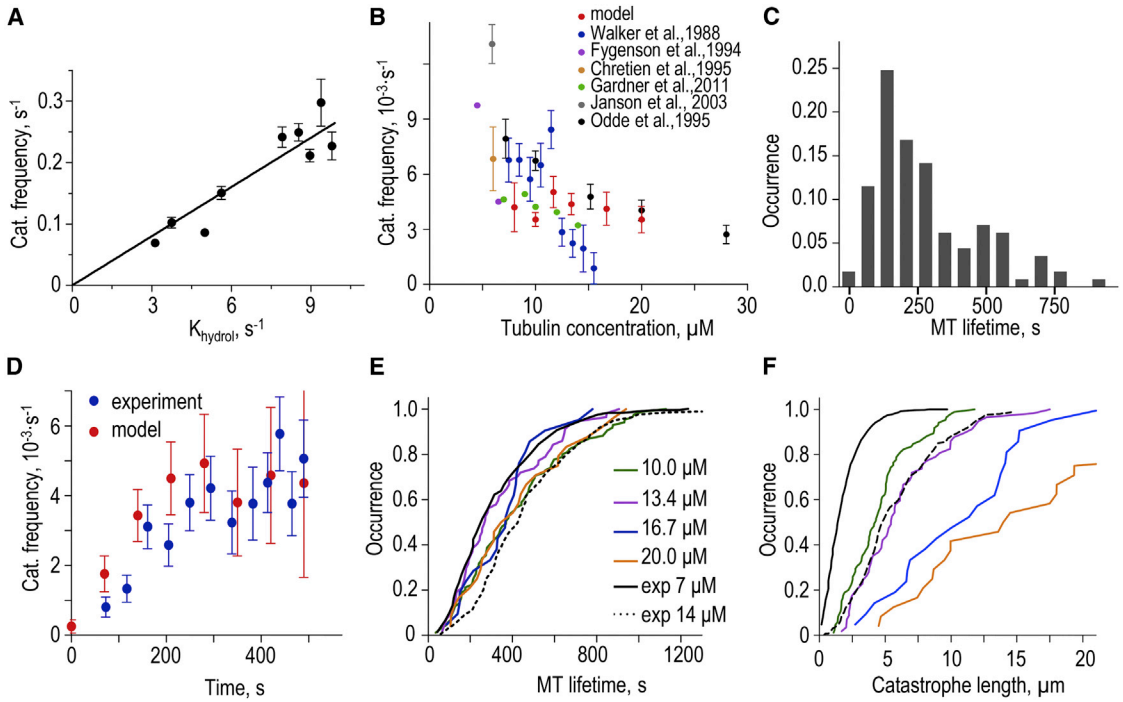

FIGURE 3 Characterization of MT aging in silico. (*A*) Calculated catastrophe frequency (mean ± SD) as a function of the GTP hydrolysis rate, K_{hydrol}. (*Solid line*) Linear fit. Total number of simulated catastrophe events for this graph $N = 551$. To analyze MT catastrophes, we routinely used $K_{\text{hydrol}} = 9\ \text{s}^{-1}$, but data were normalized to represent $K_{\text{hydrol}} = 0.11\ \text{s}^{-1}$ for all other panels in this figure. (*B*) MT catastrophe frequency versus soluble tubulin concentration. Each theoretical point is mean ± SE, based on $N = 232$ simulations. Differences in experimental data are in part due to the differences in experimental conditions. (*C*) Distribution of MT lifetimes in the model based on $N = 113$ simulations; soluble tubulin 10 μM. (*D*) Changes in MT catastrophe frequency versus time for 10 μM tubulin. Experimental data are from Gardner et al. (24). Theoretical data points were calculated using Eq. 1 in Gardner et al. (24) and our theoretical cumulative MT lifetime distribution in (*E*) for 10 μM tubulin. Theoretical error bars are SDs estimated by bootstrapping ($n = 100$ samples). (*E*) Cumulative MT lifetime distributions for different tubulin concentrations. Experimental data for two different tubulin concentrations from Gardner et al. (24). (*F*) Cumulative distributions of MT lengths at the time of catastrophe for different tubulin concentrations. See (*E*) for details. To see this figure in color, go online.

meaning that the coordinates and angles for these tubulins were fixed (Fig. 4 *A*). Thus, the dynamic changes took place only in the terminal MT fragment, which shifted continuously in the direction of MT elongation. We varied the length of this terminal fragment, so that the frozen subunits were located at least 4, 7, or 10 tubulin layers away from the tip of the shortest protofilament at any given time. Interestingly, the rates of MT growth, shortening, and catastrophe frequency were highly similar for all these calculations (Fig. 4 *B*), demonstrating that molecular and mechanical changes within the MT wall have little effect on its dynamic behavior. These results strongly suggest that the MT aging in our model is not caused by the accumulation of permanent MT wall defects.

To further test the above conclusion we sought to determine the exact time when MT commits to a catastrophe. Such task would be difficult to accomplish with the real MTs, but using a computational approach, one can step back in time from a catastrophe event and start (replay) calculations from different times before this catastrophe (20). We used tip configurations of one original MT recorded at different times before this MT's catastrophe as the starting points for new calculations, determining when the replayed MTs underwent new catastrophes. Strikingly, even if the tip configuration at the exact time of the original catastrophe was used, such replayed MTs were not doomed. The immediate catastrophe took place in only 90% of the replayed MTs (Fig. 4 *C*, time 0 s), strongly suggesting that MT catastrophe is not a deterministic event even on the subsecond timescale. This original catastrophe configuration, however, was clearly predisposed for this outcome, as the distribution of the MT lifetimes for the replayed trials from the time = 0 s configuration could be fit well with a single exponential function (Fig. 4 *D*, *red line*). When MT configurations from earlier times before the original catastrophe were used, the fraction of the replayed MTs that underwent immediate catastrophe dropped quickly. For example, almost all MTs with the tip configuration that was observed 11 s before the original catastrophe continued to polymerize upon the replay (Fig. 4 *C*, time = −11 s). Consistently, the distributions of the MT lifetimes generated for large precatastrophe times could not be fit with single exponential functions, while simulations that started from the

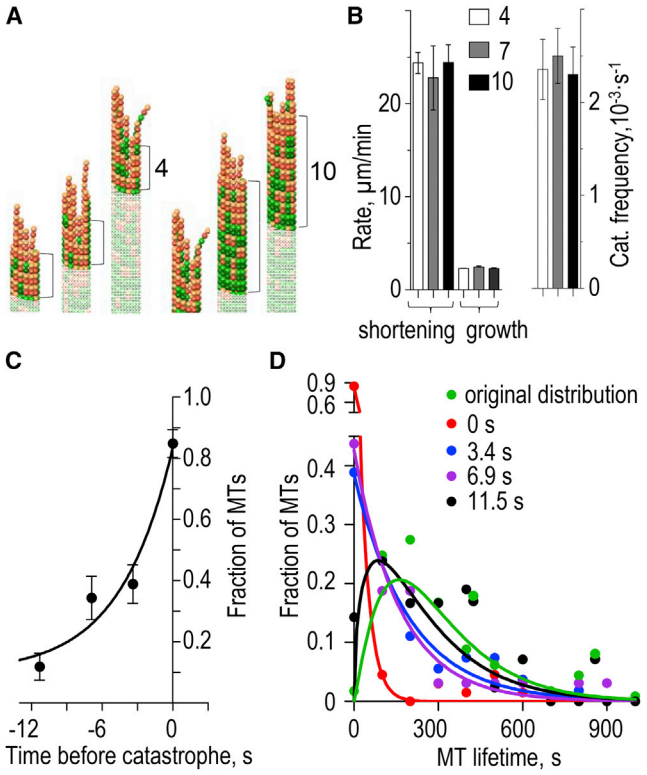

FIGURE 4 Analysis of the MT wall's role in promoting catastrophe in silico. (*A*) Illustrations for two calculation schemes in which different portions of the MTs were frozen (*pale color*). Numbers corresponds to the full layers of tubulin dimers. Calculations were carried out for these layers and their variable protofilament extensions (*bright colors*). These images are for MT growth with $K_{hydrol} = 0.5\ s^{-1}$. Similar schemes were employed to calculate the rate of shortening and catastrophe frequency. (*B*) Parameters of dynamic instability calculated for MTs with different lengths of terminal segments, as illustrated for 4 and 10 layers in (*A*). Each column (mean ± SE) is based on 9–14 polymerizing MTs, 7–16 depolymerizing MTs, and 53–70 catastrophes. (*C*) Fraction of the MTs that underwent catastrophe during first 0.5 s from the start of replay calculations. First, a routine MT simulation was carried out using a blunt MT seed as a starting configuration. After this original MT experienced a catastrophe, the exact time of this original catastrophe event was set as 0. Next, the MT tip configurations at this time and at 3, 7, and 11 s before the original catastrophe (indicated with negative numbers on the *horizontal graph axis*) were used as the starting configurations for replay calculations to determine whether these MT tips were already predisposed to catastrophe. Results are the averages of $N = 70$ replay calculations for each time point. Error bars are SDs estimated by bootstrapping (n = 32–66 samples). (*Line*) Exponential fit with characteristic decay time 4.2 s; this time is very short, indicating that MT catastrophe is not driven by MT wall defects. (*D*) Histogram distributions of the MT lifetimes generated from replay calculations starting at the indicated times before original catastrophe, and the steady-state original distribution (same as in Fig. 3 *C*). To see this figure in color, go online.

configuration at −11 s led to a lifetime distribution that was highly similar to the original (Fig. 4 *D*, *green* versus *black*). Together, these results argue strongly against the slow accumulation of permanent defects in the MT walls, and indicate that the stochastic events that lead to catastrophe are confined to the MT tip.

Tapering of a growing MT tip in this model does not change considerably during the lifetime of MT

We then examined whether in our MT model the tip changed progressively during MT growth, as predicted by the model in Coombes et al. (41). The difference in length between the shortest and the most protruding protofilaments in the MT tip, referred to as the "tip extension", was used as a measure of tip-tapering. Fig. 5 *A* shows that the tip extension of an individual MT end is highly variable; it initially increases but plateaus ~2 s after the initiation of polymerization. However, protofilament protrusions remain relatively short during the entire lifetime of the MT: at 10–20 μM soluble tubulin concentration, the mean tip extension at steady state is ~60–90 nm or 8–12 tubulin dimers. These extensions are similar to those seen at the polymerizing MT ends with cryo-electron microscopy (30); moreover, the MT increment lengths measured with low force in vitro are also matched well with this model (see Fig. S1 *C* and Schek et al. (55)). Importantly, our MT model does not predict the unbounded increase in tip extension during MT lifetime, in contrast to Coombes et al. (41). To test this conclusion further, we examined the behavior of the tips of three different MTs, which had the same number of GTP tubulins but their tips differed in shape: tapered, slightly ragged as in a typical MT polymerizing at steady state in our model, and a blunt tip as in the MT seed (see Movie S4). Fig. 5 *B* illustrates that during tubulin assembly, the blunt and tapered tips evolve to adopt the configurations with mean tip extensions as in the ragged MTs at steady state. Thus, the shape of the MT tip in this model is robust: the tips tend to reach a stationary level of raggedness regardless of the initial tip configuration, implying that such tip structure is energetically favorable.

We have also compared the extent and kinetics of MT end tapering in our model and in experimental studies of MT tips with electron and fluorescent microscopy. Model predictions are in tune with several studies that report an increase in protofilament extensions when MTs polymerize in the presence of increasing tubulin concentration (Fig. 5 *C*) (31,41,56). Different experimental approaches, however, disagree on the kinetics of tapering in MTs over time for a constant tubulin concentration. The prediction of this model that the tapering increases within seconds from the beginning of polymerization but then remains constant (Fig. 5 *A*) is inconsistent with conclusions in Coombes et al. (41), but it is in tune with results in Chrétien et al. (31). Indeed, our analysis of the electron microscopy measurements of Chrétien et al. (31) found no statistically significant changes in the tip extensions of MTs sampled at different times from the start of polymerization (see Appendix SE and Fig. S5). While the exact kinetics of MT tip tapering in vitro remain controversial, it is clear that the age-dependent MT catastrophe in our model cannot be attributed to the slow evolution of the MT tip structure.

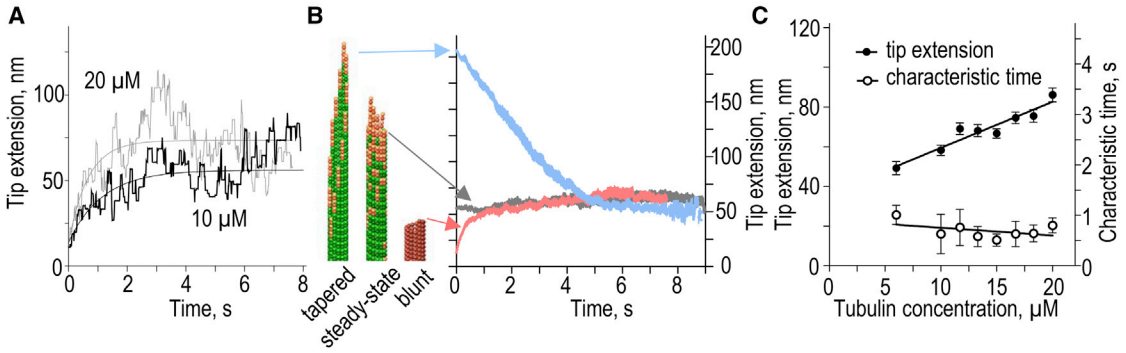

FIGURE 5 Evolution of protofilament extensions at the growing MT tip. (*A*) MT tip extensions (difference between the shortest and the longest protofilaments) as a function of time for two representative simulations. (*Smooth lines*) Exponential fits. (*B*) Evolution of the MT tip extensions in simulations that started from different initial tip configurations: tapered, steady-state (as in Fig. 2 *C*) and blunt (MT seed). Each curve is the mean of $N = 32$ simulations. (*C*) Characteristic time to achieve a steady state for tip extension length during MT assembly and the steady-state tip extension length. Data are mean ± SE based on $N = 32$ simulations for each tubulin concentration; lines are linear fits. To see this figure in color, go online.

MT with no GTP-cap is metastable if the tip is blunt, lacking the curled protofilament protrusions

To gain further insight into the mechanisms of MT catastrophe and molecular causes of aging, we then investigated the role of the GTP-cap. After beginning of a simulation from a stable seed, the size of the GTP-cap in our model increased quickly, and in 4–7 s it reached a steady state with 8–10 tubulin layers enriched in GTP-tubulins, corresponding to the total of ~120 GTP-tubulins per MT end (10 μM tubulin, Figs. 2 *C* and 6 *A*). The exact size of the GTP-cap in MTs in vitro is not known, but our theoretical prediction lies within the range of the experimental as well as other theoretical estimates (7,15,20,57,58). The GTP-cap size increased in the model proportionally to tubulin concentration, but the characteristic time of cap formation did not change appreciably (1.9 ± 0.1 s for 10 μM tubulin; Fig. 6 *B*). The model could also match well the experimental dependency of EB1 comet size on tubulin concentration, assuming that the comet size was simply proportional to the number of GTP-tubulins (see Fig. S1 *D* and Appendix SB).

To probe the stabilizing properties of the GTP-cap, we next modeled a dilution experiment by simulating a sharp drop in soluble tubulin concentration after the MT has polymerized for some time. In the absence of soluble tubulin, the MTs underwent catastrophes, but the onset of MT shortening was delayed. The range of the lag times before the catastrophes as a function of tubulin concentration in silico was highly similar to the experiment in vitro (Fig. 6 *C*) (26,27), so the model describes the dilution experiment without additional assumptions or parameter changes. Interestingly, after removal of soluble tubulin in silico, the MT stopped elongating immediately and switched into a phase of slow shortening (Fig. 6, *D* and *E*). During this phase, tubulin dimers and short protofilament protrusions dissociated from the MT tip in the absence of the simultaneous loss of the lateral bonds between all protofilaments, the hallmark of the postcatastrophic MT shortening (see Movie S5). During this slow shortening phase, the GTP-containing cap decayed exponentially (Fig. 6, *D* and *E*), as expected for random GTP hydrolysis. Surprisingly, the catastrophe commenced only 1.7 ± 0.5 s after a loss of most of the GTP dimers, indicating that the capless MT is metastable. Previous experimental work has suggested that MT metastability can be associated with the blunt geometry of the MT tip (59). Consistently, in our model the slow shortening tended to pause briefly if the tip lacked the curled protofilament protrusions, delaying the onset of catastrophic shortening (see Movie S5). To further test this hypothesis, we calculated the delay time before catastrophe using the GDP-MTs with two different tip configurations: with a blunt end (see Movie S6), and with 13 curled protofilaments, as in a typical depolymerizing MT. The latter MT disassembled immediately after the start of simulation (<0.1 s, $N = 32$), while the catastrophic shortening of the capless blunt MT took place ~2 s later ($N = 32$), consistent with a marked metastability of this tip configuration.

Curled protofilaments tend to destabilize the MT and predispose it to catastrophe

The results described in the previous section imply that the conformation of protofilament extensions at the MT tip, not just the GTP-cap, play an important role in controlling the onset of catastrophic MT shortening. They also suggest that curled protofilaments may represent a catastrophe-promoting factor. To test this hypothesis, we examined polymerization from the MT tips that lacked GTP-caps completely but contained different numbers and arrangements of curled GDP-protofilaments. When soluble tubulin was present, the blunt tip supported continuous MT polymerization in 100% of trials (Fig. 6 *F*, configuration 1.0), consistent with its metastability in the absence of soluble tubulin. Adding one curled protofilament atop the blunt

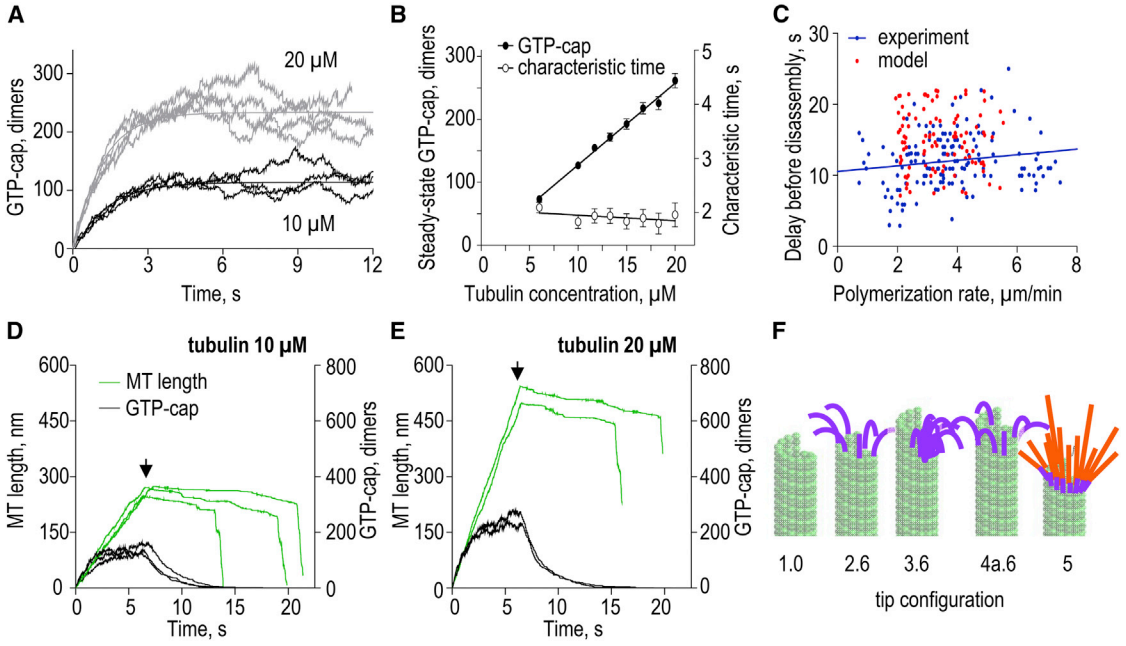

FIGURE 6 Metastability of a blunt MT tip that has no GTP-cap. (*A*) Total number of GTP-tubulin dimers in the MT as a function of time for two different tubulin concentrations. Each curve corresponds to an individual simulation; smooth lines are exponential fits to the average of the displayed curves. (*B*) Characteristic time to achieve a steady state for the GTP-cap size and the steady-state GTP-cap size. (*Data points*) Mean ± SE based on $N = 32$ simulations for each tubulin concentration; (*lines*) linear fits. (*C*) Time between removal of soluble tubulin and the onset of rapid MT disassembly as a function of the MT polymerization rate before tubulin removal. (*Solid blue line*) Linear fit to experimental points (data from Walker et al. (27)), showing no significant slope ($p = 0.052$). (*Red points*) Predicted delay times for individual MTs. Three seconds were added to the calculated delay times to mimic a relatively slow removal of tubulin in experiments in vitro. (*D*) Typical length-versus-time plots for three MTs growing at 10 μM tubulin in silico. Tubulin concentration was set to zero after 6.5 s of growth (*arrow*). Number of GTP-tubulin dimers (*black curves*) for the same MTs is plotted on the right axis. (*E*) Same simulations as in (*D*) but for two MTs growing at 20 μM tubulin. Two distinct phases of MT shortening are clearly visible in all these examples. (*F*) Schematic of MT tip configurations (numbered at the *bottom*) used to examine MT stability in 10 μM tubulin. Purple curled protofilaments had GDP-dimers as in ram's-horns. Each red protofilament had four GTP-dimers placed atop one bent GDP-dimer. See text for more details and Table 2 for the results of these simulations. To see this figure in color, go online.

MT tip did not change this outcome (Table 2, configuration 2.1, and Fig. S4). This curl broke off quickly, resulting in a blunt tip, which then elongated robustly. Even six curled extensions placed atop the every other protofilament consistently resulted in polymerization: only 1 out of 32 such MTs underwent catastrophe within 0.5 s from the start of simulation (Fig. 6 *F*, configuration 2.6). Interestingly, the effect from the same number of protofilament curls was very different when they splayed out from the blunt MT tip adjacently or intermittently with the straight GDP-tubulin protofilaments (Fig. 6 *F*, configurations 3.6 and 4a.6). Instead of promoting the rescue of curled protofilaments, the straight GDP-protofilaments became destabilized by a loss of lateral bonds on one side and these protofilaments curled rapidly (compare Movies S7 and S8). Strikingly, 70–80% of MTs with such starting configurations experienced catastrophe (Table 2). These data demonstrate that for some tip configurations, curling protofilaments can indeed exert a strong catastrophe-promoting effect even in the presence of soluble tubulin. This destabilizing activity is not caused by a different association of soluble tubulin with the tips of curled versus straight protofilaments, because our model uses the simplifying assumption that tubulin binds with equal probability to any terminal dimer, independently of its nucleotide state. Moreover, addition of straight GTP-tubulins to the tips of the curls does not improve MT stability, as demonstrated by the high catastrophe frequency predicted for the tip in which GTP-tubulin extensions were added on top of one dimer layer containing bent GDP-tubulins (Fig. 6 *F*, configuration 5; Table 2). Together, these results emphasize the importance of directly calculating the tubulin-tubulin bond energies, elastic deformations, and thermal fluctuations of protofilament protrusions, because it is difficult to guess or deduce the stability rankings for numerous configurations that arise stochastically during MT growth.

MT aging correlates with the frequency of encountering multiple curled protofilaments, but not with the kinetics of the GTP-tubulin cap

Importantly, curled tubulin protofilaments with variable nucleotide content (e.g., having a bent GDP-tubulin at the base of the protofilament plus an extension with a mixture

TABLE 2 Stability of MTs with Various Tip Configurations

Group	MT Configuration	No. of Curls at the MT Tip	Configuration No.[a]	MT Catastrophes
1	blunt GDP-MT end	0 (Movie S6)	1.0	0
2	curled GDP-protofilaments, separated by one-protofilament gaps, on top of the blunt GDP-MT end	1	2.1	0
		2 (Movie S7)	2.2	0
		4	2.4	1
		6 (Fig. 6 *F*)	2.6	1
3	adjacently located curled GDP-protofilaments splaying out from the blunt GDP-MT end	2	3.2	29
		4	3.4	29
		6 (Fig. 6 *F*)	3.6	21
		8	3.8	21
		10	3.10	26
		12	3.12	26
4a	curled GDP-protofilaments (alternating with straight GDP-protofilaments) splaying out from the blunt GDP-MT end	2 (Movie S8)	4a.2	26
		4	4a.4	23
		6 (Fig. 6 *F*)	4a.6	25
4b	curled GDP-protofilaments (alternating with two straight protofilaments that are connected with lateral bonds) splaying out from the blunt GDP-MT end	2	4b.2	20
		4	4b.4	21
5	composite protofilament extensions on top of the blunt GDP-MT; each extension has one bent GDP-tubulin and four GTP-tubulin dimers	13 (Fig. 6 *F*)	5	24
6	GTP-protofilaments (four dimers each) on top of the blunt GDP-MT end	13	6	0

Calculations started from indicated configurations in 10 μM soluble tubulin, and the fate of MTs was examined 0.5 s later ($K_{hydrol} = 9\ s^{-1}$). Numbers for MT catastrophes in the last column are based on $N = 32$ trials for each configuration. Curled protofilaments contained four GDP-tubulin dimers. Group 2 had curled protofilaments added on top of the blunt GDP-MT end; in groups 3 and 4, the curled protofilaments splayed out in different arrangements from the blunt GDP-MT ends. Protofilament extensions in groups 5 and 6 contained four GTP-tubulins, so these segments were straight. Calculations for group 6 started with the straight protofilaments initially separated with cracks (no lateral bonds), but these protofilaments adhered to each other immediately, healing the cracks and preventing MT catastrophe. In Group 5, each straight GTP-protofilament segment was positioned on top of one bent GDP-tubulin dimer (i.e., forming 0.2 rad with the GDP-tubulin belonging to the top layer of blunt GDP-MT end). The layer of bent GDP-tubulins tilted the straight GTP-protofilaments, so their adhesion was unlikely (Fig. 6 *F*, configuration 5). See Fig. S4 for detailed diagrams of all tip configurations. Movies in the Supporting Material illustrate behavior of the indicated tip configurations but in calculations with no soluble tubulin, so the difference in stability is evident from the duration of lags before catastrophic shortening.

[a]See Figs. 6 *F* and S4.

of GDP- and GTP-tubulins) are found occasionally at the tips of polymerizing MTs in our model, so we hypothesize that such curls may represent the short-lived repairable defects of the MT tip. Their number at the polymerizing MT tips fluctuates considerably, sometimes reaching the maximal value of 13 (Fig. 7 *A*). Consistent with the above analyses, even 10–13 protofilament curls do not necessarily trigger a catastrophe because these destabilizing defects can repair quickly, as the curls break off and the new GTP-tubulins are added in their place (see Movies S1 and S3). Interestingly, the number of GTP tubulins in the cap also fluctuates significantly (Fig. 7 *B*), and occasionally the cap disappears completely in simulations with accelerated GTP hydrolysis, because in this case the total number of GTP subunits is very low. Many of such events also do not result in catastrophe, likely because of the metastability of certain tip configurations. The rapid kinetics of the GTP-cap size and the number of protofilament curls do not correlate with each other, emphasizing the remarkable complexity and stochasticity of the MT tip system. To study in more details the molecular events preceding MT catastrophe, we synchronized these data for $N = 52$ simulated MTs using the time of their catastrophes (enlarged in *insets* in Fig. 7, *A* and *B*). Interestingly, we found no significant trends in the size of the GTP-cap immediately before or after catastrophe. In contrast, the number of the protofilament curls at the MT tip increased rapidly just before the onset of catastrophic shortening. Thus, MT catastrophe is preceded by the transient formation of multiple curled protofilaments but not by the loss of GTP-tubulin cap.

With this insight we sought to examine whether the stochastic fluctuations in the number of curled protofilaments at the growing MT tip correlated with MT aging, which takes place on a much longer timescale relative to the catastrophe-preceding molecular events. Strikingly, the probability to encounter a large number of curled protofilaments at the growing MT tip increased slowly over the lifetime of the MT (Fig. 7 *C*). Moreover, the timing for this increase was similar to the kinetics of MT aging (Fig. 3 *D*). In contrast, the average size of the GTP-cap in the same MTs reached the steady state much more rapidly, and the size of the cap did not change during the subsequent MT growth. Thus, the gradual increase in the probability to encounter a fluctuation with the large number of curled protofilaments

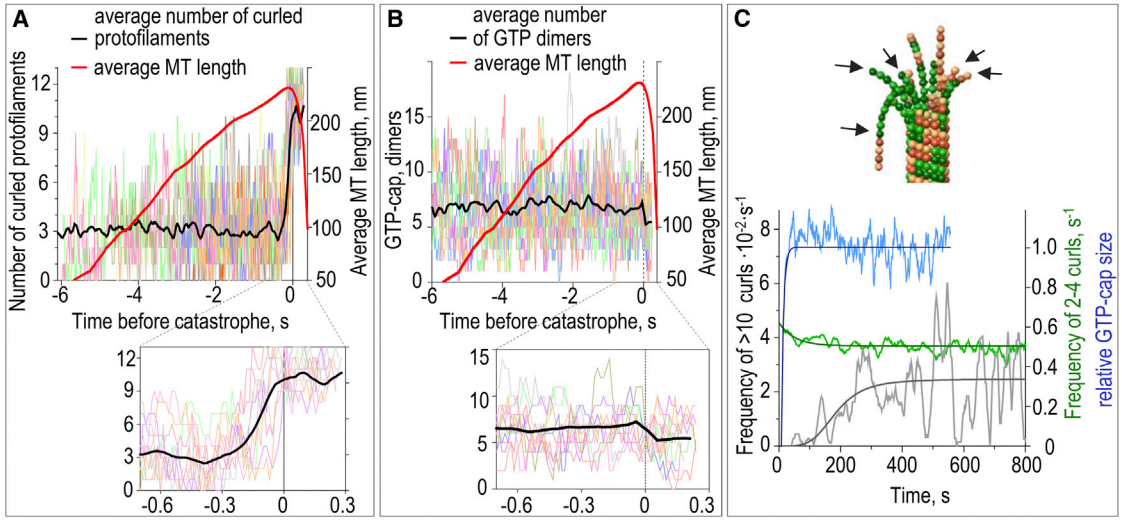

FIGURE 7 Transient fluctuation in the number of curled protofilaments as a catastrophe-promoting factor. (*A*) Kinetics of the formation of protofilament curls (*left axis*) before the catastrophe. (*Thin colored lines*) Number of curled protofilaments in 10 individual MTs synchronized at the time of catastrophe (time 0). (*Thick black line*) Average number of protofilament curls based on $N = 52$ simulations. (*Thick red line*) Average length of these MTs (*right axis*), so the onset of shortening at time 0 is evident. (*Inset*) Zoom of a 0.9-s time window encompassing catastrophe. Data in (*A*) and (*B*) are for $K_{hydrol} = 9\ s^{-1}$. (*B*) Kinetics of the GTP-cap size before the catastrophe. (*Thin colored lines*) Number of GTP-tubulin dimers in the same in silico experiments as in (*A*); see legend to (*A*) for more details. (*Thick black line*) Average number of GTP-tubulins. (*C*) Top image is an example of the growing MT tip ($K_{hydrol} = 0.5\ s^{-1}$) with numerous protofilament curls that have variable nucleotide content (*arrows*). Graph below shows the kinetics of changes in MT tip configurations from the start of polymerization: the frequency of encountering ≥ 10 protofilament curls (in *gray*, *left axis*), frequency of encountering 2–4 protofilament curls (in *green*, *right axis*), and the relative size of the GTP-cap (in *blue*, *right axis*). (*Variable curves* in *lighter colors*) Average data from $N = 79$ simulated MTs. (*Thick smooth lines*) Best fits based on exponential functions (for *green* and *blue curves*). (*Fitting curve* in *black*) Sigmoidal Hill function: $C \times t^h/(\tau^h + t^h)$, where $C = 2.9 \times 10^{-3}\ s^{-1}$, $\tau = 185.4 \pm 50.4$ s, and $h = 4.2$. To see this figure in color, go online.

can explain the asymptotic increase in the MT catastrophe frequency during tubulin assembly.

DISCUSSION

Brownian dynamics modeling of tubulin-tubulin interactions

Molecular nature of the sudden transitions between phases of tubulin assembly and disassembly remain one of the most enigmatic aspects of MT physiology. Previous experimental studies have provided compelling evidence for the importance of the GTP-tubulin cap in governing MT catastrophe. However, it has not been possible to recapitulate in a quantitative manner the full spectrum of experimental observations of MT behavior in vitro within the frame of a single theory using one set of parameters, indicating the significant gaps in knowledge. Many of these discrepancies between the experiment and modeling became exposed recently, thanks to a renewed interest in MT aging (11,24,40,41). Here, we have extended previous modeling efforts in this field to build a realistic molecular-mechanical model to study the causes of MT catastrophe and aging. To our knowledge, our model is the first to take advantage of the Brownian dynamics approach, accelerated by a supercomputer and parallel programming. Importantly, the model has no thermodynamic penalties or predetermined rules for tubulin dimers dissociation depending on their specific location or the identity of neighboring subunits within the tip. The key simplifying assumptions in the model posit that 1) GTP hydrolysis is random; 2) bond energies and protofilament stiffness do not change after GTP hydrolysis; and 3) GDP-tubulins in the MT wall tend to form curled protofilaments or ram's-horns. Despite these and other simplifications (see Materials and Methods), this modeling framework is sufficient to provide a robust match to major experimental MT observations in vitro, including 1) typical rates for MT disassembly and assembly for 6–20 μM tubulin concentration range (Fig. 2, *A*, *B*, *G*, and *H*); 2) characteristic shapes of the shortening and growing MT tips (Fig. 2, *C–F*), including MT increment lengths and EB1 comet length (see Fig. S1, *C* and *D*); 3) quantitative features of MT aging (Fig. 3, *C–F*); 4) weak dependence of the catastrophe rate on soluble tubulin concentration (Fig. 3 *B*); and 5) the delay times before MT catastrophe after sudden tubulin dilution (Fig. 6 *C*). The results of the previous theoretical analyses of the force development by depolymerizing MT also remain valid (34,39). We explain this modeling success by our use of Langevin equations of motion, which represent adequately a tremendous complexity of the molecular events that underlie MT dynamics and stability. Even relatively simple two-state models using macroscopic rate constants can mimic the kinetics of MT growth and shortening (11,21), but describing a wider range of quantitative

dependencies appears to require the explicit incorporation of the impact of thermal motions on tubulin protofilament mechanics and on the stability of tubulin-tubulin bonds.

This modeling approach should benefit from future refinements, because some of the model simplifications may be limiting. Most notably, current computer technology does not allow calculating MT dynamics within a reasonable timeframe using a realistic rate of GTP hydrolysis. We overcame this technical limitation by using the accelerated rate of GTP hydrolysis, but future analysis should aim to incorporate a physiological GTP hydrolysis rate, requiring ~20-fold increase in computational power. Another notable simplification in this model is that protofilament bending is limited by two dimensions (in the plane of the protofilament), preventing examination of more complex tip configurations, such as multiprotofilament protrusions and sheets. We estimate that incorporating realistic three-dimensional motions of tubulin assemblies will require an approximately fivefold additional increase in computing speed. Removing these limitations should expand the application range of this model but it is unlikely to change current conclusions significantly, because this model demonstrates a solid match to several key experimental dependencies and this comprehensive description is internally consistent. Importantly, analysis of MT behavior using this model has already led, to our knowledge, to new insights into the molecular mechanisms of catastrophe and has provided a conceptually novel view of MT aging, as discussed below.

MT catastrophe as a stochastic fluctuation of the conformation and composition of tubulin protofilament extensions

The canonical model for the molecular causes of MT catastrophe postulates that loss of the GTP-containing tubulin cap exposes GDP-tubulin core of the MT, which is inherently unstable and undergoes unavoidable, catastrophic shortening (1,3,8) (Fig. 8 *A*). Assuming that GTP hydrolysis is random with the rate constant 0.5 s^{-1} (45), the probability to lose all GTP-tubulin subunits at the MT tip is vanishingly small and requires years to observe, while the characteristic time to observe MT catastrophe in vitro is on the order of minutes. This discrepancy suggests that either the GTP-cap is much smaller than what is expected with random GTP hydrolysis or the MT catastrophe can take place even when the GTP-cap loss is incomplete but exceeds some threshold. This notion and the apparent inability of past models with random GTP hydrolysis to recapitulate some key experimental dependencies have focused previous theoretical efforts on identifying specific GTP hydrolysis rules, e.g., induced or vectorial (11), which would provide a better experimental description. It is interesting in this respect that our model performed well despite our simplifying assumption that GTP hydrolysis is entirely random. This does not argue against the idea that GTP is hydrolyzed with a different rate in some tubulins, but prohibiting GTP hydrolysis in the terminal dimers in our model did not change its behavior significantly (not shown), so this feature does not appear to be essential.

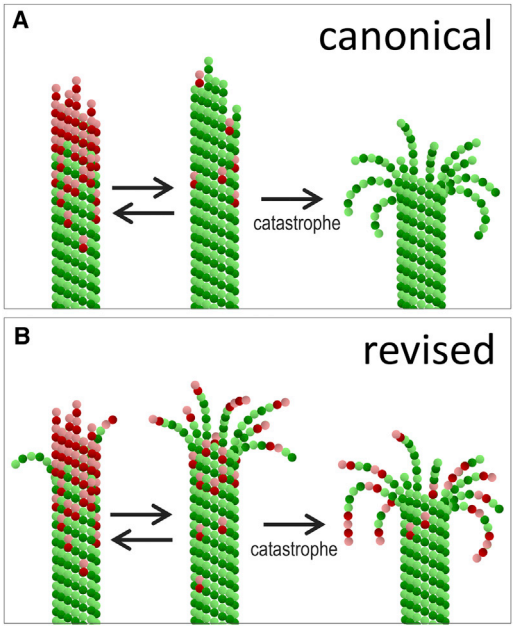

FIGURE 8 Proposed mechanism of MT catastrophe and aging. (*A*) Simplified schematics of the canonical mechanism to explain MT catastrophe. This mechanism emphasizes the stochasticity in the number and location of the GTP-tubulin dimers at the MT tip. The complete or partial loss of the GTP-cap in this model leads to imminent catastrophe, followed by the curling of protofilaments and MT shortening. (*B*) Simplified schematics of the proposed mechanism underlying MT catastrophe. This study modifies the canonical view by demonstrating that in addition to the randomness of GTP-tubulin content, MT stability is strongly affected by stochastic fluctuations in the conformation of a growing MT tip. In this view, the catastrophe is a rare random fluctuation of multiple molecular and mechanical tip features, among which the protofilament curls may represent a major catastrophe-promoting factor. Aging of the MT is an emerging property of a complex stochastic system, representing fluctuating MT tip, to evolve slowly toward the steady-state level of the occurrence of configurations with the higher frequency of protofilament curls and therefore higher catastrophe probability. To see this figure in color, go online.

We also do not find evidence for a specific GTP-cap size threshold. In the model, a smaller GTP-cap is more prone to catastrophe (Figs. 3 *A* and S3 *B*), fully consistent with its overall importance. However, even the complete loss of GTP tubulins is not sufficient to trigger catastrophe, as seen from the lack of imminent catastrophes of blunt MTs in the presence of soluble tubulin (Table 2), and from the 1–2 s lag between the loss of GTP-tubulins and catastrophic shortening in simulated dilution experiments (Fig. 6, *D* and *E*, and Movies S5 and S6). These results strongly indicate that other features of the MT end, not just its GTP content, govern the probability to catastrophe. This conclusion is consistent with theoretical findings in Margolin et al. (20); however, unlike in this previous model, the precatastrophe

MT tips in our model do not have the laterally unbonded segments (cracks) between protofilaments. In the molecular-mechanical model, which incorporates thermal protofilament motions, the cracks are unstable and they heal quickly, as seen from the lack of catastrophes in MT that have a GTP-cap in which all GTP protofilaments are initially not bonded (Table 2, configuration 6). Instead, the MT catastrophes in our model correlate with the conformation of protofilament protrusions, which are highly variable during MT growth. Indeed, with no protrusions, the blunt end of the capless GDP-MT does not undergo catastrophe in the presence of soluble tubulin because this metastable configuration is readily rescued by addition of new GTP-tubulin subunits. However, the MT end that has multiple splayed protofilaments is highly unstable even if it has high GTP-tubulin content. Moreover, adding straight GTP-tubulins on top of the already kinked GDP subunits increases MT stability only slightly, because the probability that thermal noise straightens several protofilaments simultaneously, allowing them to adhere to each other, is very low (compare stability of MT tip configurations 5 and 6, Table 2). Importantly, during normal MT assembly, the configuration of the tip fluctuates quickly and continuously, exhibiting not only different GTP-tubulin content but also marked variability in the number, length, and conformation of protofilament protrusions (Fig. 7, *A* and *B*). We propose that in real MT, as in our model, MT catastrophe results from the rare coincidences of such multiple stochastic molecular and mechanical features, most important of which is the thermally and mechanically induced bending of protofilaments away from the MT cylinder (Fig. 8 *B*).

Evolution of the short-lived reversible molecular events at the MT tip underlies the MT aging

In our model the MT exhibits aging, i.e., a slow asymptotic increase in catastrophe frequency during the first few minutes of MT elongation, in a quantitatively similar manner to what is seen in vitro (24). Yet, we ruled out the previously proposed causes of MT aging, which postulated the accumulation of visible permanent alterations in either the MT wall or tip (Fig. 1, *A* and *B*). Our analysis also shows that the catastrophe in the model is a highly stochastic, nondeterministic event up until the commencement of rapid shortening. Indeed, even the MT configuration that was found at the start of the catastrophe in one MT, is not fully committed, as using this configuration to start new calculations leads to catastrophe in only ~90% of trials (Fig. 4 *C*). This situation creates a paradox, in which the highly dynamic and stochastic MT tip appears to have a memory of a previous MT lifetime. This memory lasts for minutes (Fig. 3, *C* and *D*), while the characteristic timescale of the elementary processes associated with the MT assembly is much shorter. For example, tubulin subunits exchange at the MT tip in the model and in vitro on the millisecond timescale. A similarly short time characterizes the tubulin-tubulin bond dissociation, while the characteristic time of GTP hydrolysis is on the order of seconds, which is still much faster than MT aging. A common perception of aging is that it is accompanied by the accumulation of permanent features, i.e., lasting from the time of their appearance until the process ends, so the mismatch between the slow aging of the MT as a whole and the transient nature of molecular events at the tip is not intuitive. There is, however, no paradox in this mismatch, because, in complex stochastic systems, the short-lived events can affect a system's behavior on a much longer timescale. We illustrate this idea with a simplified stochastic model, in which a system (a highly simplified representation of the MT tip) can undergo reversible transitions between N different states, while transition into a final state is irreversible (mimicking a catastrophe) (Fig. 9 *A* and Appendix SF). We further hypothesize that each transition adds temporarily a specific molecular feature to the MT tip, which can be called a repairable defect, although we avoid using this term because we believe that these transient features reflect natural variability of the molecular events at the MT tip. It is easy to see that when $N = 1$, the catastrophe in this scheme is a single-step process and the distribution of MT lifetime is described with exponential function. When $N = 3$ and the time of backward transitions is infinitely large, this scheme corresponds to the previously proposed 3-hits model, in which three permanent, irreversible defects trigger a catastrophe (11,24). The distribution of MT lifetimes in this case is nonexponential, and it fits well the experimental MT lifetime distribution (Fig. 9 *B*). A similarly good fit, however, can be obtained with this scheme using multiple parameter sets corresponding to numerous reversible transitions. Importantly, the elementary transition time decreases with the increasing system's complexity as $1/N^2$ (Fig. 9 *C*). Thus, the nonexponential distribution of MT lifetimes can simply arise owing to the complexity of the MT tip, which quickly acquires and loses different highly transient molecular features. During the MT assembly, the probabilities for the occurrence of different transient features change gradually toward their specific steady states with different characteristic times (Fig. 9 *D*). In this sense, MT aging is an emerging property of the complex system, representing a fluctuating MT tip, to evolve slowly and asymptotically toward the steady-state levels of occupancy for some rare destabilizing configurations. Our analysis shows that these destabilizing configurations cannot be described in simple terms, as we could not find any prominent visible features that were typical for precatastrophe MT tips. However, the model predicts that the frequency of the configurations with a large number of curled protofilament protrusions changes over time with kinetics similar to the observed changes in catastrophe frequency (Fig. 7 *C*). Because protofilament curls represent a strong catastrophe-promoting factor, and there is a stochastic increase in their number

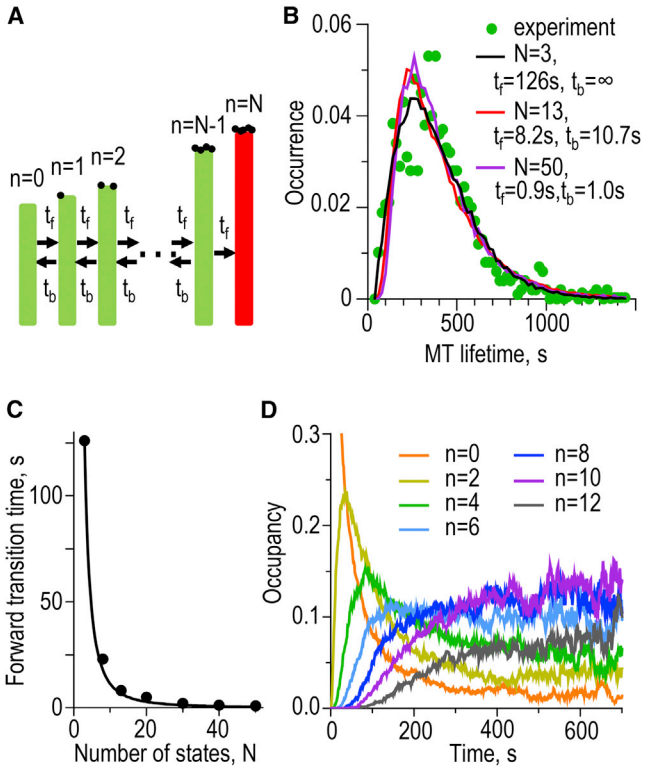

FIGURE 9 A simplified stochastic model to illustrate MT aging. (*A*) Schematic of the simplified MT model, in which N different states of the tip are connected with reversible transitions (*arrows*). (*Black dots* at the *tip*) Molecular features (i.e., defects); each transition either adds or removes one feature. Transition from state $(N-1)$ to state N is irreversible, mimicking catastrophe. (*B*) Experimental distribution of MT lifetimes from Gardner et al. (24) and theoretical model fits with three parameter sets, which differ in the total number of states N and transition times. The infinitely large backward transition time for $N = 3$ corresponds to irreversible transitions. For $N > 3$, the best fit is obtained when the ratio t_b/t_f lies in the 1.0–1.3 range, so the underlying defects are highly reversible. (*C*) Time for a forward transition t_f as a function of the total number of states N for the parameter sets that match well the experimental distribution of MT lifetimes. (*Black line*) Fitting with $t_f \sim 1/N^2$. (*D*) Kinetics of the occupancy of different states during calculations that started from the state with $n = 0$ features (S_0 state, see Appendix SF); $N = 13$, $t_f = 12.5$ s, and $t_b = 20$ s. Occupancy of the initial state with zero features decreases exponentially. The occupancy of states with larger number n of reversible features increases with the progressively slower kinetics. The slow kinetics for the occurrence of final state (catastrophe) in this simplified model indicates the system's aging. This is analogous to the slow kinetics of the occurrence of fluctuations with the large number of protofilament curls in the molecular-mechanical MT model (Fig. 7 *C*). To see this figure in color, go online.

immediately prior catastrophe, we propose that slow change in this transient and short-lived feature (the lifetime of the protofilament curls at the growing MT tip is <100 ms) represents a molecular cause of MT aging. Future computational analysis should examine this hypothesis in detail, seeking the accurate and quantitative predictor for the probability of a growing MT tip to switch into rapid shortening.

Our study reveals the importance of thermal and mechanical deformations of the protofilament protrusions in determining quantitative characteristics of MT dynamics. In the future, this major new insight, will hopefully assist the analyses of the mechanisms of action of different agents that affect MT stability. In the frame of this model, the MT-associated proteins that stabilize and increase the length of curled protofilaments at the ends of growing MT should promote catastrophe, while factors that reduce the lifetime of these transient curls are expected to stabilize MT growth. Simultaneously accelerating the GTP hydrolysis rate and increasing the occurrence of curled protofilaments may have synergistic effect, as indeed suggested by the recent study that combined MT-destabilizing agent vinblastine with the EB proteins (60). We hope that the developed theoretical model will promote detailed mechanistic investigations of the mechanisms of action of different MT-binding proteins and drugs.

SUPPORTING MATERIAL

Six Appendices, five figures, and eight movies are available at http://www.biophysj.org/biophysj/supplemental/S0006-3495(15)01156-X.

AUTHOR CONTRIBUTIONS

F.I.A. and E.L.G. designed research; P.Z., N.G., and F.I.A. performed research; V.V. and A.T. provided essential computing tools; P.Z., N.G., F.I.A., and E.L.G. analyzed data; and E.L.G., F.I.A., and N.G. wrote the article.

ACKNOWLEDGMENTS

We are grateful to Maxim Molodtsov for his help in the initial phase of this work, and A. Zaytsev for help with preparing materials for publication. We thank Drs. Y. Goldman, P. Tran, D. Odde, and T. Surrey for fruitful discussions.

This work was supported in part by grants from the National Institutes of Health to E.L.G. (grant No. GM-R01098389) and from the Presidium of the Russian Academy of Sciences program No. 1 to F.I.A. and by the Supercomputing Center of Lomonosov Moscow State University. E.L.G. is supported in part by a Research Scholar Grant (No. RSG-14-018-01-CCG) from the American Cancer Society. N.G. is supported by a Dynasty Foundation Fellowship and the RF President's grant for young scientists.

SUPPORTING CITATIONS

References (61–67) appear in the Supporting Material.

REFERENCES

1. Desai, A., and T. J. Mitchison. 1997. Microtubule polymerization dynamics. *Annu. Rev. Cell Dev. Biol.* 13:83–117.
2. McIntosh, J. R., V. Volkov, …, E. L. Grishchuk. 2010. Tubulin depolymerization may be an ancient biological motor. *J. Cell Sci.* 123:3425–3434.
3. Mitchison, T., and M. Kirschner. 1984. Dynamic instability of microtubule growth. *Nature.* 312:237–242.
4. Horio, T., and H. Hotani. 1986. Visualization of the dynamic instability of individual microtubules by dark-field microscopy. *Nature.* 321: 605–607.

5. Carlier, M. F., D. Didry, and D. Pantaloni. 1987. Microtubule elongation and guanosine 5′-triphosphate hydrolysis. Role of guanine nucleotides in microtubule dynamics. *Biochemistry.* 26:4428–4437.
6. Erickson, H. P., and E. T. O'Brien. 1992. Microtubule dynamic instability and GTP hydrolysis. *Annu. Rev. Biophys. Biomol. Struct.* 21:145–166.
7. O'Brien, E. T., W. A. Voter, and H. P. Erickson. 1987. GTP hydrolysis during microtubule assembly. *Biochemistry.* 26:4148–4156.
8. Howard, J., and A. A. Hyman. 2009. Growth, fluctuation and switching at microtubule plus ends. *Nat. Rev. Mol. Cell Biol.* 10:569–574.
9. Alushin, G. M., G. C. Lander, …, E. Nogales. 2014. High-resolution microtubule structures reveal the structural transitions in $\alpha\beta$-tubulin upon GTP hydrolysis. *Cell.* 157:1117–1129.
10. Brouhard, G. J. 2015. Dynamic instability 30 years later: complexities in microtubule growth and catastrophe. *Mol. Biol. Cell.* 26:1207–1210.
11. Bowne-Anderson, H., M. Zanic, …, J. Howard. 2013. Microtubule dynamic instability: a new model with coupled GTP hydrolysis and multistep catastrophe. *BioEssays.* 35:452–461.
12. Chen, Y. D., and T. L. Hill. 1985. Monte Carlo study of the GTP cap in a five-start helix model of a microtubule. *Proc. Natl. Acad. Sci. USA.* 82:1131–1135.
13. Bayley, P., M. Schilstra, and S. Martin. 1989. A lateral cap model of microtubule dynamic instability. *FEBS Lett.* 259:181–184.
14. Flyvbjerg, H., T. E. Holy, and S. Leibler. 1994. Stochastic dynamics of microtubules: a model for caps and catastrophes. *Phys. Rev. Lett.* 73:2372–2375.
15. van Buren, V., D. J. Odde, and L. Cassimeris. 2002. Estimates of lateral and longitudinal bond energies within the microtubule lattice. *Proc. Natl. Acad. Sci. USA.* 99:6035–6040.
16. van Buren, V., L. Cassimeris, and D. J. Odde. 2005. Mechanochemical model of microtubule structure and self-assembly kinetics. *Biophys. J.* 89:2911–2926.
17. Molodtsov, M. I., E. A. Ermakova, …, F. I. Ataullakhanov. 2005. A molecular-mechanical model of the microtubule. *Biophys. J.* 88:3167–3179.
18. Brun, L., B. Rupp, …, F. Nédélec. 2009. A theory of microtubule catastrophes and their regulation. *Proc. Natl. Acad. Sci. USA.* 106:21173–21178.
19. Padinhateeri, R., A. B. Kolomeisky, and D. Lacoste. 2012. Random hydrolysis controls the dynamic instability of microtubules. *Biophys. J.* 102:1274–1283.
20. Margolin, G., I. V. Gregoretti, …, H. V. Goodson. 2012. The mechanisms of microtubule catastrophe and rescue: implications from analysis of a dimer-scale computational model. *Mol. Biol. Cell.* 23: 642–656.
21. Hill, T. L. 1984. Introductory analysis of the GTP-cap phase-change kinetics at the end of a microtubule. *Proc. Natl. Acad. Sci. USA.* 81:6728–6732.
22. Pantaloni, D., and M. F. Carlier. 1986. Involvement of guanosine triphosphate (GTP) hydrolysis in the mechanism of tubulin polymerization: regulation of microtubule dynamics at steady state by a GTP cap. *Ann. N. Y. Acad. Sci.* 466:496–509.
23. Caplow, M. 1992. Microtubule dynamics. *Curr. Opin. Cell Biol.* 4: 58–65.
24. Gardner, M. K., M. Zanic, …, J. Howard. 2011. Depolymerizing kinesins Kip3 and MCAK shape cellular microtubule architecture by differential control of catastrophe. *Cell.* 147:1092–1103.
25. Walker, R. A., E. T. O'Brien, …, E. D. Salmon. 1988. Dynamic instability of individual microtubules analyzed by video light microscopy: rate constants and transition frequencies. *J. Cell Biol.* 107:1437–1448.
26. Voter, W. A., E. T. O'Brien, and H. P. Erickson. 1991. Dilution-induced disassembly of microtubules: relation to dynamic instability and the GTP cap. *Cell Motil. Cytoskeleton.* 18:55–62.
27. Walker, R. A., N. K. Pryer, and E. D. Salmon. 1991. Dilution of individual microtubules observed in real time in vitro: evidence that cap size is small and independent of elongation rate. *J. Cell Biol.* 114:73–81.
28. Bayley, P. M., M. J. Schilstra, and S. R. Martin. 1990. Microtubule dynamic instability: numerical simulation of microtubule transition properties using a lateral cap model. *J. Cell Sci.* 95:33–48.
29. Martin, S. R., M. J. Schilstra, and P. M. Bayley. 1993. Dynamic instability of microtubules: Monte Carlo simulation and application to different types of microtubule lattice. *Biophys. J.* 65:578–596.
30. Mandelkow, E. M., E. Mandelkow, and R. A. Milligan. 1991. Microtubule dynamics and microtubule caps: a time-resolved cryo-electron microscopy study. *J. Cell Biol.* 114:977–991.
31. Chrétien, D., S. D. Fuller, and E. Karsenti. 1995. Structure of growing microtubule ends: two-dimensional sheets close into tubes at variable rates. *J. Cell Biol.* 129:1311–1328.
32. Grishchuk, E. L., M. I. Molodtsov, …, J. R. McIntosh. 2005. Force production by disassembling microtubules. *Nature.* 438:384–388.
33. Akiyoshi, B., K. K. Sarangapani, …, S. Biggins. 2010. Tension directly stabilizes reconstituted kinetochore-microtubule attachments. *Nature.* 468:576–579.
34. Volkov, V. A., A. V. Zaytsev, …, E. L. Grishchuk. 2013. Long tethers provide high-force coupling of the Dam1 ring to shortening microtubules. *Proc. Natl. Acad. Sci. USA.* 110:7708–7713.
35. Grishchuk, E. L., J. R. McIntosh, …, F. I. Ataullakhanov. 2012. Force generation by dynamic microtubule polymers. *In* Comprehensive Biophysics. Elsevier, New York, pp. 93–117.
36. Caplow, M., R. L. Ruhlen, and J. Shanks. 1994. The free energy for hydrolysis of a microtubule-bound nucleotide triphosphate is near zero: all of the free energy for hydrolysis is stored in the microtubule lattice. *J. Cell Biol.* 127:779–788.
37. Wang, H.-W., and E. Nogales. 2005. Nucleotide-dependent bending flexibility of tubulin regulates microtubule assembly. *Nature.* 435:911–915.
38. Molodtsov, M. I., E. L. Grishchuk, …, F. I. Ataullakhanov. 2005. Force production by depolymerizing microtubules: a theoretical study. *Proc. Natl. Acad. Sci. USA.* 102:4353–4358.
39. Efremov, A., E. L. Grishchuk, …, F. I. Ataullakhanov. 2007. In search of an optimal ring to couple microtubule depolymerization to processive chromosome motions. *Proc. Natl. Acad. Sci. USA.* 104:19017–19022.
40. Odde, D. J., L. Cassimeris, and H. M. Buettner. 1995. Kinetics of microtubule catastrophe assessed by probabilistic analysis. *Biophys. J.* 69:796–802.
41. Coombes, C. E., A. Yamamoto, …, M. K. Gardner. 2013. Evolving tip structures can explain age-dependent microtubule catastrophe. *Curr. Biol.* 23:1342–1348.
42. Voevodin, V. V., S. A. Zhumatiy, …, V. V. Voevodin. 2012. Practice of "Lomonosov" supercomputer. *Open Systems Publ. (Moscow).* 7: 36–39.
43. Castle, B. T., and D. J. Odde. 2013. Brownian dynamics of subunit addition-loss kinetics and thermodynamics in linear polymer self-assembly. *Biophys. J.* 105:2528–2540.
44. Müller-Reichert, T., D. Chrétien, …, A. A. Hyman. 1998. Structural changes at microtubule ends accompanying GTP hydrolysis: information from a slowly hydrolyzable analogue of GTP, guanylyl (α,β)methylenediphosphonate. *Proc. Natl. Acad. Sci. USA.* 95:3661–3666.
45. Melki, R., S. Fievez, and M. F. Carlier. 1996. Continuous monitoring of P_i release following nucleotide hydrolysis in actin or tubulin assembly using 2-amino-6-mercapto-7-methylpurine ribonucleoside and purine-nucleoside phosphorylase as an enzyme-linked assay. *Biochemistry.* 35:12038–12045.
46. Ermak, D. L., and J. A. McCammon. 1978. Brownian dynamics with hydrodynamic interactions. *J. Chem. Phys.* 69:1352–1360.
47. Brouhard, G. J., and L. M. Rice. 2014. The contribution of $\alpha\beta$-tubulin curvature to microtubule dynamics. *J. Cell Biol.* 207:323–334.

48. Buey, R. M., J. F. Díaz, and J. M. Andreu. 2006. The nucleotide switch of tubulin and microtubule assembly: a polymerization-driven structural change. *Biochemistry.* 45:5933–5938.

49. Kononova, O., Y. Kholodov, …, V. Barsegov. 2014. Tubulin bond energies and microtubule biomechanics determined from nanoindentation in silico. *J. Am. Chem. Soc.* 136:17036–17045.

50. Grafmüller, A., and G. A. Voth. 2011. Intrinsic bending of microtubule protofilaments. *Structure.* 19:409–417.

51. McIntosh, J. R., E. L. Grishchuk, …, F. I. Ataullakhanov. 2008. Fibrils connect microtubule tips with kinetochores: a mechanism to couple tubulin dynamics to chromosome motion. *Cell.* 135:322–333.

52. Tran, P. T., P. Joshi, and E. D. Salmon. 1997. How tubulin subunits are lost from the shortening ends of microtubules. *J. Struct. Biol.* 118: 107–118.

53. Dimitrov, A., M. Quesnoit, …, F. Perez. 2008. Detection of GTP-tubulin conformation in vivo reveals a role for GTP remnants in microtubule rescues. *Science.* 322:1353–1356.

54. Gildersleeve, R. F., A. R. Cross, …, R. C. Williams, Jr. 1992. Microtubules grow and shorten at intrinsically variable rates. *J. Biol. Chem.* 267:7995–8006.

55. Schek, H. T., 3rd, M. K. Gardner, …, A. J. Hunt. 2007. Microtubule assembly dynamics at the nanoscale. *Curr. Biol.* 17:1445–1455.

56. Gardner, M. K., B. D. Charlebois, …, D. J. Odde. 2011. Rapid microtubule self-assembly kinetics. *Cell.* 146:582–592.

57. Seetapun, D., B. T. Castle, …, D. J. Odde. 2012. Estimating the microtubule GTP cap size in vivo. *Curr. Biol.* 22:1681–1687.

58. Maurer, S. P., N. I. Cade, …, T. Surrey. 2014. EB1 accelerates two conformational transitions important for microtubule maturation and dynamics. *Curr. Biol.* 24:372–384.

59. Tran, P. T., R. A. Walker, and E. D. Salmon. 1997. A metastable intermediate state of microtubule dynamic instability that differs significantly between plus and minus ends. *J. Cell Biol.* 138:105–117.

60. Mohan, R., E. A. Katrukha, …, A. Akhmanova. 2013. End-binding proteins sensitize microtubules to the action of microtubule-targeting agents. *Proc. Natl. Acad. Sci. USA.* 110:8900–8905.

61. Demchouk, A. O., M. K. Gardner, and D. J. Odde. 2011. Microtubule tip tracking and tip structures at the nanometer scale using digital fluorescence microscopy. *Cell. Mol. Bioeng.* 4:192–204.

62. Zhang, B., J. Zerubia, and J.-C. Olivo-Marin. 2007. Gaussian approximations of fluorescence microscope point-spread function models. *Appl. Opt.* 46:1819–1829.

63. Bieling, P., L. Laan, …, T. Surrey. 2007. Reconstitution of a microtubule plus-end tracking system in vitro. *Nature.* 450:1100–1105.

64. Fygenson, D. K., E. Braun, and A. Libchaber. 1994. Phase diagram of microtubules. *Phys. Rev. E Stat. Phys. Plasmas Fluids Relat. Interdiscip. Topics.* 50:1579–1588.

65. Janson, M. E., M. E. de Dood, and M. Dogterom. 2003. Dynamic instability of microtubules is regulated by force. *J. Cell Biol.* 161:1029–1034.

66. Laue, T., and B. Demeler. 2011. A postreductionist framework for protein biochemistry. *Nat. Chem. Biol.* 7:331–334.

67. Vitre, B., F. M. Coquelle, …, I. Arnal. 2008. EB1 regulates microtubule dynamics and tubulin sheet closure in vitro. *Nat. Cell Biol.* 10:415–421.

SUPPORTING MATERIALS

MOLECULAR AND MECHANICAL CAUSES OF MICROTUBULE CATASTROPHE AND AGING

Pavel Zakharov[1], Nikita Gudimchuk[2,3,4], Vladimir Voevodin[3], Alexander Tikhonravov[3], Fazoil I. Ataullakhanov[2,3,4] and Ekaterina L. Grishchuk[1]

[1]Department of Physiology, Perelman School of Medicine, University of Pennsylvania, Philadelphia, USA 19104
[2]Center for Theoretical Problems of Physicochemical Pharmacology, Russian Academy of Sciences, Moscow, Russia 119991
[3]Moscow State University, Moscow, Russia 119899
[4]Federal Research Center of Pediatric Hematology, Oncology and Immunology, Moscow Russia 117198

Appendix A. Calculating gradients of the total MT energy

The derivative of the total energy of the system with respect to independent variables $q^i_{k,n}$ is given by the following equation:

$$\frac{\partial U_{total}}{\partial q^i_{k,n}} = \frac{\partial v^{lat}_{k,n}}{\partial q^i_{k,n}} + \frac{\partial v^{inter}_{k,n}}{\partial q^i_{k,n}} + \frac{\partial v^{intra}_{k,n}}{\partial q^i_{k,n}} + \frac{\partial g^{bending}_{k,n}}{\partial q^i_{k,n}} \quad \text{(Eq. S1)}$$

It includes terms corresponding to the lateral interactions, inter and intra longitudinal interactions between tubulin subunits and the bending energy (see Eqs. 1-5 in *Materials and Methods*). To accelerate calculations we used explicit analytical expressions for all energy gradients:

$$\begin{cases} \frac{\partial v^{lat}_{k,n}}{\partial q^i_{k,n}} = \left(A_{lat} \cdot \frac{r^{lat}_{k,n}}{r_0^2} \cdot \exp\left(\frac{-r^{lat}_{k,n}}{r_o}\right) \cdot \left(2 - \frac{r^{lat}_{k,n}}{r_o}\right) + \frac{2 \cdot b_{lat} \cdot r^{lat}_{k,n}}{d \cdot r_o} \cdot \exp\left(\frac{-\left(r^{lat}_{k,n}\right)^2}{d \cdot r_o}\right) \right) \cdot \frac{\partial r^{lat}_{k,n}}{\partial q^i_{k,n}} \\ \frac{\partial v^{intra}_{k,n}}{\partial q_k} = k \cdot r_{k,n} \cdot \frac{\partial r_{k,n}}{\partial q^i_{k,n}} \\ \frac{\partial g^{bending}_{k,n}}{\partial q^i_{k,n}} = \frac{\partial g^{bending}_{k,n}}{\partial \chi_{k,n}} \cdot \frac{\partial \chi_{k,n}}{\partial q^i_{k,n}} = B \cdot \left(\chi_{k,n} - \chi_o\right) \cdot \frac{\partial \chi_{k,n}}{\partial q^i_{k,n}} \end{cases} \quad \text{(Eq. S2)}$$

See *Materials and Methods* and *Table 1* for details. The gradient for inter-dimer longitudinal bond was written analogously to the gradient for lateral bond.

Appendix B. Determining parameters of MT dynamic instability from theoretical data and other model analyses

The output of numerical calculations, i.e. the coordinates and angles of tubulin monomers as a function of time, were analyzed using custom-written MATLAB programs (2012b, MathWorks). MT length at each time was defined as the average z-coordinate of the most distant dimers in each protofilaments. The onset of MT growth was defined as the time point when MT length increased by at least 20 nm. Introducing this rule was necessary for a consistent comparison between MT starting from a blunt "seed" and MT re-growing from the "seed" after a previous cycle of polymerization-depolymerization. Often, MTs depolymerized incompletely, leaving the residual protofilament curls less than 20 nm in length, so the growth was assumed to take place when MT length exceeded the 20 nm threshold.

Polymerization rate was calculated as a slope of the length vs. time dependency smoothed by applying 80 ms moving average. The depolymerization phase was defined as the time period during which the MT length decreased by at least 32 nm (8 monomer layers). Thus, fluctuations in the MT length less than 8 monomer layers were attributed to the variability in MT length during its growth, rather than to depolymerization and rescue. MT catastrophe time was defined using an automated algorithm written in MATLAB (Fig. S2B inset). MT rescues were infrequent, consistent with a rare occurrence of these events in vitro.

Fluctuations in MT length were calculated as the length increments for a leading protofilament during simulated MT growth with 0.1 s sampling intervals, as in experiments with low force in (55) (Fig. S1C). EB comet profiles were simulated via a convolution of the calculated GTP-tubulin dimer distribution with the Gaussian point-spread function corresponding to 512 nm emission wavelength of GFP (61, 62). EB comet size was calculated as the characteristic length of the resulting exponentially decaying profile. A good match to data in (63) was obtained for $K_{hydrol,} = 0.11\ s^{-1}$, same value as used elsewhere in the paper for model comparison with experimental data; other model parameters were as in Table 1 (Fig. S1D).

Appendix C. Normalizing results of the calculations with accelerated rate of GTP hydrolysis

The catastrophe frequency in our model is proportional to K_{hydrol} in the range from 3 to 11 s^{-1} (Fig. 3A), implying that modeling results obtained with high hydrolysis rates can be used to study MT catastrophes at normal hydrolysis rate 0.1 - 0.5 s^{-1} (7, 45), which are not computationally accessible with current tools. When the linear fit in Fig. 3A is extrapolated to this hydrolysis rate range, the predicted catastrophe frequency is $(3 - 15)\cdot 10^{-3}\ s^{-1}$, similar to the experimental range (24, 25, 31, 40, 64, 65). Differences in the reported catastrophe frequencies often reflect different experimental conditions, such as buffer composition or temperature. Unless stated otherwise, theoretical results reported here have been scaled to represent $K_{hydrol,} = 0.11\ s^{-1}$, because this value provides the best match to experimental catastrophe frequency $(3 - 3.5)\cdot 10^{-3}\ s^{-1}$ reported in (24), where MT aging was studied in details. Specifically, data obtained in our model with $K_{hydrol} = 9\ s^{-1}$ were normalized by "slowing down" the modeling time by a factor of 82 (ratio of the accelerated to experimental hydrolysis rate constants) prior to plotting (Fig. 3 panels B-F, Fig. 4 panel B catastrophe frequency, Fig. 4 panels C and D, Fig. 7 panel C). When such scaling is applied to the lifetime distributions calculated using different K_{hydrol} value (Fig. S3A), the normalized distributions are similar, justifying this approach. To further test this scaling procedure we also calculated three additional model outputs: size of the cap (number of GTP subunits), characteristic time to achieve a steady state for the cap size and the frequency of encountering different number of protofilament curls. All these dependencies are described by linear functions (Fig. S3B,C; note that the reciprocals of the GTP-cap size

and characteristic time are plotted), strongly suggesting that the composition and conformation of the MT tip are scalable at different hydrolysis rate. These results also imply that the mechanisms of MT catastrophe at different hydrolysis rates are fundamentally similar.

Appendix D. Comparison of modeling parameters used in current work and in the mechanochemical models

The mechanochemical model based on the original approach developed by VanBuren et al. (16) has previously been used to predict the unbounded increase in MT tip tapering during MT growth (41), while MT tapering in our model reaches a steady-state quickly. To try to understand why these models behave differently we compared the values of model parameters, which were used to make these predictions. Consistent with the results from MT nanoindentations in silico (49), our model uses relatively strong tubulin-tubulin bonds: the lateral and longitudinal bond energies are 9.1 and 15.5 k_BT, respectively (Table 1). The mechanochemical models in (16, 41, 56) employ somewhat similar energy bond ratios, such that the lateral bond is weaker than the longitudinal one, however, these energies correspond to relatively weak interactions: 3.2 - 5.7 and 6.8 - 9.5 k_BT for the lateral and longitudinal bonds, respectively. The direct comparison between energy values in these and our model is difficult, however, because these models differ in the overall shape of tubulin energy potentials. Here, and in our previous models (17, 38, 39), we use energy potential with a well and an activation barrier (Fig. S1A), consistent with protein-protein interaction studies (66), while the energy profile in mechanochemical model is a potential well (e.g. Fig. 1B in (16)).

Other difference between two modeling approaches is our use of a much slower rate constant for tubulin addition: 8.3 $\mu M^{-1}s^{-1}$ vs. 58-65 $\mu M^{-1}s^{-1}$ per MT in more recent versions of the mechanochemical model (41, 56). Importantly, the values for this constant and the energy parameters are not user-defined, but they are determined from model calibrations, i.e. fitting the model to obtain a match to specific experimental dependencies. As described in Materials and Methods section *Choice of Model Parameters and Model Calibration*, in our model the value for $k_{on,MT,}$ is determined from the MT polymerization rate dependency in Fig. 2B. The 8.3 $\mu M^{-1}s^{-1}$ value we obtain is close to some experimental reports, e.g. (25). When the value of $k_{on,MT}$ is increased in our model without changing other parameters, the rate of MT growth increases proportionally, as expected, and it no longer matches the experimental range. Since our model does not permit a direct control over the dissociation constant k_{off}, the increase in MT polymerization rate due to a faster $k_{on,MT}$ can be compensated only indirectly, e.g. by weakening the energy of tubulin-tubulin bonds. Incorporating in our model a faster $k_{on,MT}$ together with weaker bond energies recovers the physiological MT polymerization rate at 7-8 µM soluble tubulin, but it leads to a steeper slope than in experiment (Fig. S1B). More significantly, with this set of model parameters, the rate of MT shortening in our model is predicted to be 12,000 µm/min. It appears that such unrealistically fast MT disassembly prediction is a direct consequence of a high flexural rigidity of protofilament bending in our model (300 $k_BT\ rad^{-2}$, Table 1), while the mechanochemical models use only 50-60 $k_BT\ rad^{-2}$ (16, 41). Although we have not done the exhaustive analysis of model predictions for different combinations of parameter values, we believe that it should be possible to match the experimental dependency in Fig. 2B and the physiological MT depolymerization rate within the frame of our model using weaker protofilament rigidity and tubulin-tubulin bond energies, and a faster on-rate, similar to the parameter sets employed by the mechanochemical models. However, when protofilament rigidity is reduced, our model can no longer match the results of experiments on force generation by depolymerizing MTs (33, 34). Clearly, the requirement for large protofilament rigidity is not ungrounded, because generation of the power strokes by bending protofilaments is the only known mechanism to explain large forces developed by

depolymerizing MTs in vitro (35, 49). It is a unique feature of our model, however, that it can match multiple MT experiments with one set of model parameters, which severely constrains their possible values. Indeed, values of most parameters in our model cannot be changed significantly without losing the match to at least one of the key experiments, preventing us from using parameter values that work well in other models, in which the set of matched experiments was not as broad. To conclude, our limited analysis indicates that the unbounded increase in MT end tapering, as seen with the mechanochemical model (41), could potentially result from weak tubulin-tubulin interaction energies used in that model. Without strong bonding between tubulins, protofilaments can elongate semi-independently from each other, accompanied by a linear increase in the variance of their lengths. This hypothesis, however, needs further analysis of the behavior of different models and their continued experiment-based verification.

Appendix E. Fine structure of the MT tip predicted by the current model and in vitro

Different electron microscopy (EM) techniques have previously been used to examine the ends of MTs grown in vitro, but these results are controversial. In a transmission EM study of 29 MTs (41) the tips showed a narrow variation in tip extension length, with the mean increasing linearly from ~20 to 90 nm as the MT length increased from ~1 to 4 μm (Fig. 3B in (41)). Although our predicted theoretical extension length for this tubulin concentration (60-75 nm, Fig. 5C) lies within the range reported in (41), in the model the length of tip extensions increases soon after the start of polymerization and it remains constant for all MTs longer than ~ 150 nm. In a cryo-EM study in (31), a total of 2,910 MTs were examined for 3 tubulin concentrations and at least 3 time points (Table IV in (31)). To compare these results with predictions of our model we digitized data in Figs. 8 and 9 in (31) using GetData Graph Digitizer program and built cumulative distribution functions (Fig. S5 graphs). Two-sample Kolmogorov-Smirnov test was used to carry out pairwise comparisons of distributions at different time points for each tubulin concentration (Fig. S5 tables). Normalized Kolmogorov-Smirnov statistics was calculated with parameter D:

$$D = \sqrt{\frac{N_2 N_1}{N_1 + N_2}} \max|CDF_1(x) - CDF_2(x)| \qquad \text{(Eq. S3)}$$

Here, N_1 and N_2, sample sizes for each distribution, were taken from Table IV in (31).

This analysis revealed that out of 12 pairwise comparisons of the distributions of MT tip extensions documented in (31), five pairs showed no statistically significant differences at different MT lifetimes (Fig. S5). Seven pairs were significantly different but they did not form a specific trend: three pairs had a decrease in tapering with increasing MT age and four pairs had an increase in tapering. The lack of a reliable increase in the extension length in the cryo-EM study (31) is in tune with our model's prediction. Also, as in our model, the extension length was reported to increase with increasing tubulin concentration (31), although in the model the tip extension was less sensitive to tubulin concentration (Fig. 5C). We note that more recent experiments by this group (67) reported that growing MT tips had much shorter extensions at high tubulin concentrations (median values ~20 nm for 45 μM tubulin and ~80 nm for 90 μM tubulin), suggesting that the dependence of MT tip extension on tubulin concentration in vitro is not as strong as reported previously.

Fine structure of the MT tip has also been analyzed in previous experimental studies by quantifying standard deviation of the MT tip images obtained with fluorescence microscopy (41, 56, 58, 61). These studies have concluded that protofilament protrusions increase with increasing tubulin concentration, in agreement with results of the EM study in (31) and of the current model. Coombes et al. (41) additionally

report that SDs of the MT tips increase with time (150-300 nm at 12 μM tubulin); this increase was suggested to reflect a progressive tip tapering during MT growth. In contrast, a more recent fluorescent microscopy study (58) measured the significantly lower average SD values for the growing MT tips (<145 nm at 11-38 μM tubulin), consistent with our model's predictions. This experimental study also estimates that fluorescence-based microscopy cannot resolve reliably the MT tapers shorter than 180 nm, so our predicted MT tip protrusions might be below a detection limit for this technique.

Appendix F. Simplified stochastic model of MT evolution and catastrophe

The system (MT) was assumed to have several distinct configurations or states $\{S_i\}$, characterized by specific molecular features (black dots at the MT tip in Fig. 9A). Initially, the MT was in state S_0, and transitions between all subsequent states occurred with characteristic times t_f and t_b for forward and backward transitions, respectively,

$$S_o \underset{t_b}{\overset{t_f}{\rightleftarrows}} S_1 \underset{t_b}{\overset{t_f}{\rightleftarrows}} \ldots \xrightarrow{t_f} S_N \qquad \text{(Eq. S4)}$$

For a given time step *dt*, the probability of a transition *P* was calculated as

$$P_{f/b} = 1 - \exp(-dt / t_{f/b}) \qquad \text{(Eq. S5)}$$

Here, $t_{f/b}$ is the ratio of the forward to backward time constants. The script for calculations was written in MATLAB 2012; time step *dt* was selected at least 10-fold shorter than the smallest time constant. Using Eq. S5, 1000 simulations were carried out to determine MT lifetime, i.e. the total time for the system to transit from initial S_0 state to final S_N state. Multiple parameter sets (N, t_f, t_b) can provide a good match between this model and the experimental bell-shaped distribution of the MT lifetime (Fig. 9B). Importantly, the larger number of states N enables the faster transitions (i.e. short-lived evens) (Fig. 9C). Thus, this model illustrates that in complex stochastic systems, the time to reach the last "catastrophe" state (state with n=12 in Fig. 9D) can be two orders of magnitude slower than the characteristic time of individual transitions. MT aging can, therefore, represent a property of a complex stochastic system (MT tip) to approach gradually the steady state for the occurrence of the large number of short-lived features that promote MT catastrophe (black dots at the MT tip in state (N-1) in Fig. 9A). Unlike the permanent "hits" (model with N=3, Fig. 9B), in models with large Ns the short-lived "defects" are repairable, i.e. they arise and disappear continuously, so the MT aging represents the kinetics of the increase in probability to encounter these infrequent features, rather than their continuous accumulation.

Supplemental References

61. Demchouk, A.O., M.K. Gardner, and D.J. Odde. 2011. Microtubule Tip Tracking and Tip Structures at the Nanometer Scale Using Digital Fluorescence Microscopy. Cell. Mol. Bioeng. 4: 192–204.

62. Zhang, B., J. Zerubia, and J.-C. Olivo-Marin. 2007. Gaussian approximations of fluorescence microscope point-spread function models. Appl. Opt. 46: 1819–1829.

63. Bieling, P., L. Laan, H. Schek, E.L. Munteanu, L. Sandblad, M. Dogterom, D. Brunner, and T. Surrey. 2007. Reconstitution of a microtubule plus-end tracking system in vitro. Nature. 450: 1100–1105.

64. Fygenson, D.K., E. Braun, and A. Libchaber. 1994. Phase diagram of microtubules. Phys. Rev. E. 50: 1579–1588.

65. Janson, M.E., M.E. de Dood, and M. Dogterom. 2003. Dynamic instability of microtubules is regulated by force. J. Cell Biol. 161: 1029–1034.

66. Laue, T., and B. Demeler. 2011. A postreductionist framework for protein biochemistry. Nat. Chem. Biol. 7: 331–334.

67. Vitre, B., F.M. Coquelle, C. Heichette, C. Garnier, D. Chrétien, and I. Arnal. 2008. EB1 regulates microtubule dynamics and tubulin sheet closure in vitro. Nat. Cell Biol. 10: 415–421.

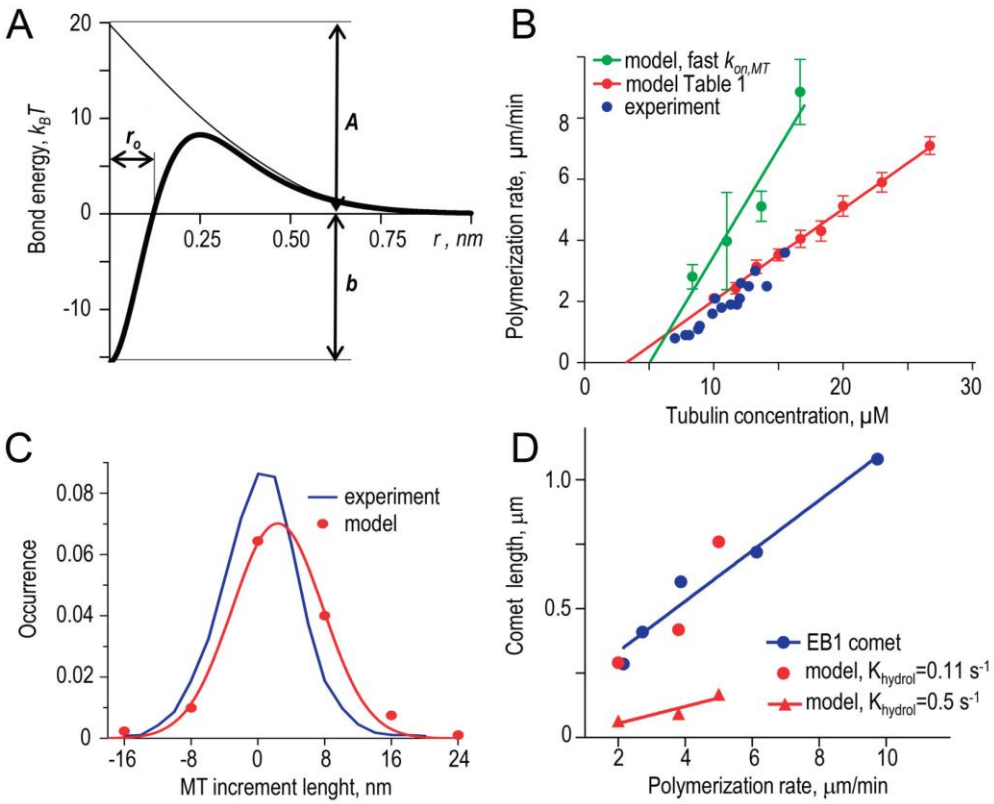

Figure S1. Quantitative analyses of the growing MT end

A. Potential energy profile for tubulin-tubulin interactions (lateral bonds and longitudinal inter-dimer bonds) used in this model. Exponent (thin line) is the first term in Eq. 1; *r* is distance between interaction points. See Fig. 1C and Table 1 for details.

B. Dependence of the MT growth rate on soluble tubulin concentration. Experimental data are from (25). Predictions of the current model with parameters listed in Table 1 are in red (same graph as in Fig. 2B). Green dots are predictions of the current model with parameters listed in Table 1 except the following changes: $k_{on,MT}$ = 58 µM s^{-1}, b_{lat} = 4.7 k_BT, b_{inter} = 9.5 k_BT, A_{lat} = 4.3 k_BT, A_{inter} = 4.8 k_BT. Each theoretical data point is the mean of 8-16 repeats, bars are SDs. Lines are liner fits to theoretical data.

C. Normalized histograms of increment lengths during MT polymerization. Experimental distribution is based on data in Fig. 5 in (55). Red dots are predictions of the current model for 6 µM tubulin (N=960) with parameters listed in Table 1, red line is Gaussian fitting. SDs for MT length increments are 4.5 and 5.4 nm for experiment and model, respectively.

D. Size of the "comets" at the growing MT ends as a function of MT polymerization rate. Experimental data are for the comet tail lengths formed by EB1 homolog Mal3 (data from Fig. 2c in (63)). Model predictions are for parameter values in Table 1 and two different GTP hydrolysis rates.

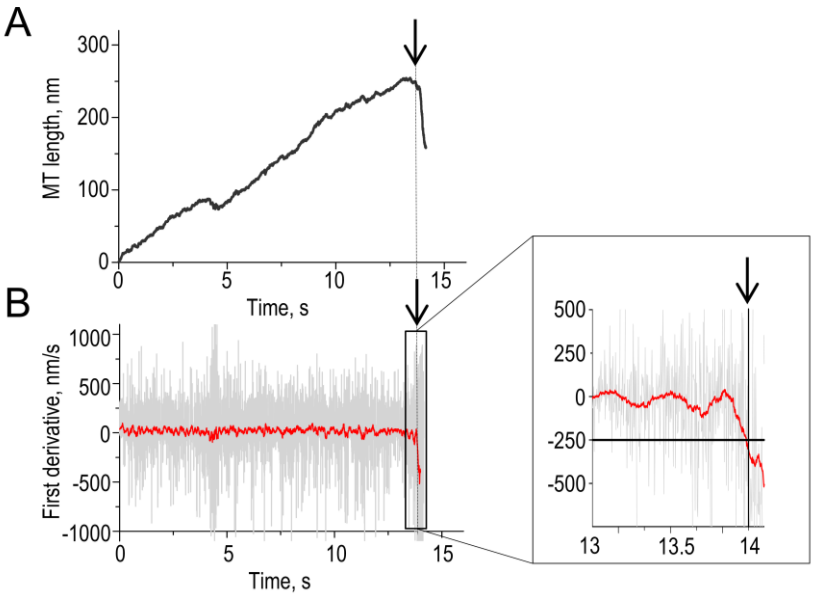

Figure S2. Algorithm to determine the time of MT catastrophe.

A. Example simulation in which MT length is plotted vs. model time (with no normalization). Data were sampled with 2 ms interval, shown after applying 80 ms moving average. Arrow points to catastrophe. Soluble tubulin concentration 10 µM, K_{hydrol} = 9 s^{-1}.

B. First derivative of the curve in panel A was calculated prior to (in grey) or after (in red) smoothing with a moving average. Inset shows enlargement of the last ~ 1 s of the simulation, revealing the onset of rapid shortening. The catastrophe time (arrow) was defined as the time point when the rate of depolymerization reached -250 nm/s (15 µm/min, horizontal black line in inset graph) and shortening continued for at least 8 monomer layers.

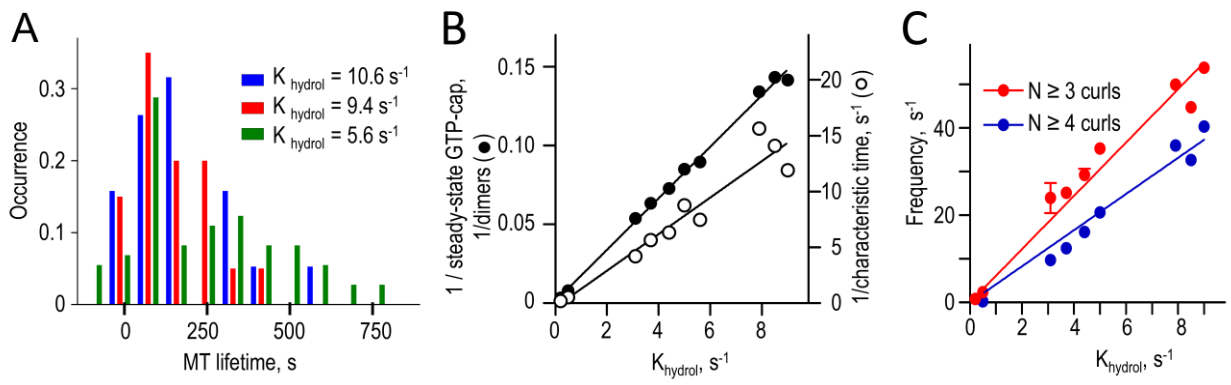

Figure S3. Scaling of model outputs calculated with different GTP hydrolysis rate.

A. Normalized distributions of MT lifetimes for different hydrolysis constants. Histograms are based on the results of N = 73, 19 and 20 simulations with K_{hydrol} = 5.6, 9.4 and 10.6 s^{-1}, respectively. Lifetimes obtained in these simulations were normalized using multiplication factor K_{hydrol}/ 0.11 s^{-1} before plotting.
B. Steady-state GTP-cap size and the corresponding characteristic time (reciprocal values are plotted) as a function of the GTP hydrolysis rate based on at least 32 simulations for each rate. Lines are linear fits for calculations with accelerated K_{hydrol} (> 3 s^{-1}). Unlike with catastrophe frequency, the size of the cap and its characteristic time can also be calculated with the realistic hydrolysis rate (shown for 0.5 s^{-1}). Importantly, the direct calculations with this slow rate and the linear extrapolation for accelerated hydrolysis rate lead to highly similar values, validating the scaling approach.
C. Frequency to encounter a given number of protofilament curls at the MT end growing at steady state as a function of the GTP hydrolysis rate. See legend to panel B for more details.

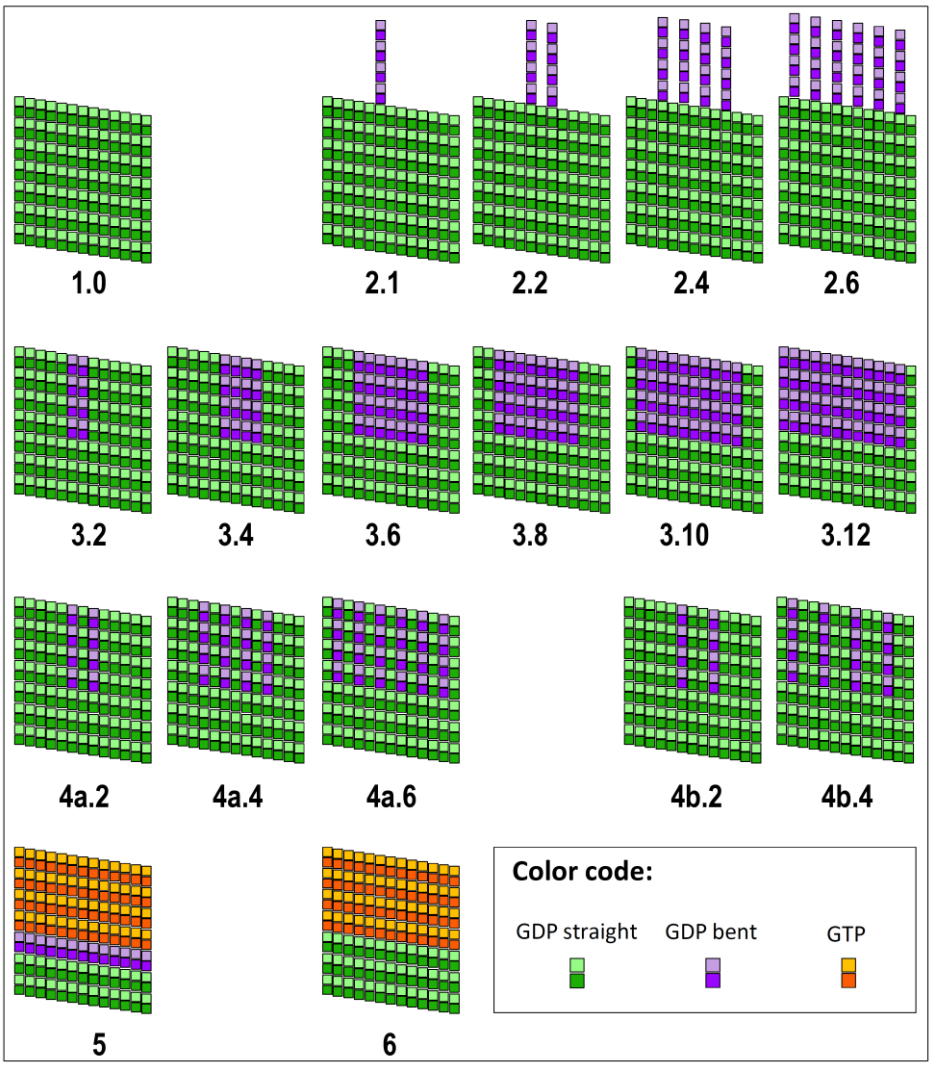

Figure S4. Diagrams of MT tip configurations used for calculations reported in Table 2.

Selected tip structures (flat representation), which were used as starting configurations for calculations with 10 μM tubulin. Different shades show α and β tubulin monomers. Leftmost protofilament in each diagram adheres to the rightmost protofilament to close into helical MT cylinder. Note that configurations in groups 3 and 4 have some straight protofilaments that lack lateral bonds with at least one neighbor, while in group 2 all straight protofilaments have lateral bonds, explaining the dramatically different stabilities of these configuration groups.

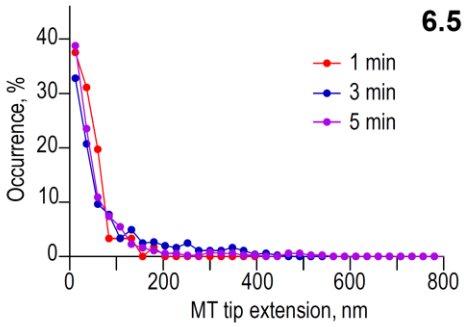

Pair for comparison	D	significance level (α)
1 min vs 3 min	1.82	** (p<0.005)
1 min vs 5 min	1.10	NS (p> 0.1)
3 min vs 5 min	1.57	* (p<0.05)

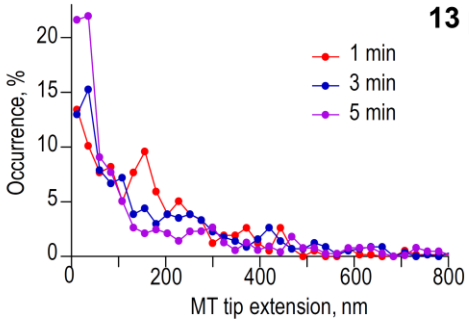

Pair for comparison	D	significance level (α)
1 min vs 3 min	1.03	NS (p> 0.1)
1 min vs 5 min	2.26	*** (p<0.001)
3 min vs 5 min	2.64	*** (p<0.001)

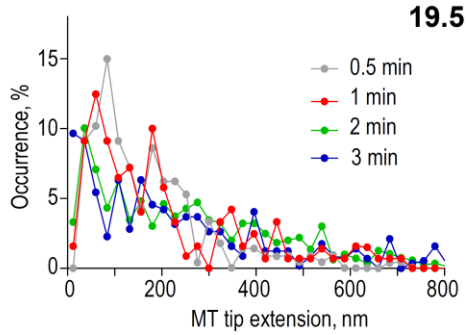

Pair for comparison	D	significance level (α)
0.5 min vs 1 min	1.18	NS (p> 0.1)
0.5 min vs 2 min	3.18	*** (p<0.001)
0.5 min vs 3 min	2.44	*** (p<0.001)
1 min vs 2 min	1.86	** (p<0.005)
1 min vs 3 min	1.35	NS (p> 0.1)
2 min vs 3 min	1.05	NS (p> 0.1)

Figure S5. Statistical analysis of MT tip extension distributions reported in (31).

Histogram distributions of the extension lengths observed at the ends of MTs that polymerized for indicated time and at indicated soluble tubulin concentration. These graphs were built by digitizing the corresponding distribution reported in Figs. 8 and 9 in (31). D was calculated with Eq. S3 (Appendix E); $D < 1.36$ means no significant difference ($p > 0.05$). Parameter α is a significance level at which null hypothesis of distributions' equality is rejected. NS – not significant.